Final report

1.1 Project details

Project title	Optimerede Layouts for Vindmølleparker i Komplekst Terræn
Project identification (program abbrev. and file)	EUDP-2013-KINASAMARBEJDE, Journal nr.: 64013-0405
Name of the programme which has funded the project	EUDP
Project managing company/institution (name and address)	DTU Wind Energy Nils Koppels Allé, Building 403, 2800 Lyngby
Project partners	Department of Wind Energy, Technical University of Denmark (DTU Wind Energy) EMD International A/S 2 Chinese partners: Power China North-West Investigation and Design Institute (NWI) and HoHai University (HHU)
CVR (central business register)	30060946, 27491529
Date for submission	March 26, 2018

1.2 Short description of project objective and results

English

The objective of the project is to develop wind farm optimization tools to optimally build wind farms in complex terrain, e.g. mountainous areas, and to integrate the tools into the Danish commercial software WAsP and WindPRO. The logic behind the Sino-Danish collaboration is to explore and use the Danish wind technology in Chinese complex terrain.

The main results from the project are:

- Measurements with 2 met-masts and strain-gauges in a turbine tower were performed in the Chinese Jingbian wind farm with 25 turbines. One-year measurement data and SCADA data were received.
- Wind farm layout optimization tools have been further developed for wind farms in complex terrain.
- The Jingbian wind farm in complex terrain has been optimized with the new tools with an AEP increase of 1.46%.
- The new version of WindPRO and WAsP (WAsP-CFD) were shown to give better wind resource predictions than the old version WAsP (>10%) and some existing CFD based commercial software (>3%).
- Optimization tools have been integrated into WindPRO and WAsP and a new version is ready to be released.

Dansk

Projektets formål er at udvikle optimeringsværktøjer til layout-optimering når der planlægges vindmølleparker i komplekst terræn, dvs. bjergområder, herudover at integrere værktøjerne i dansk kommerciel software (WAsP og WindPRO). Ideen bag det dansk-kinesiske samarbejde er at videreudvikle og anvende dansk vindteknologi i komplekst terræn i Kina.

De vigtigste resultater fra projektet er

- Målinger med 2 metmaster og belastningsmåler i et mølletårn blev udført i den kinesiske Jingbian vindmøllepark med 25 møller. Der er modtaget et års måledata og SCADA-data.
- Optimering af vindmølleparkoptimeringsværktøjer er blevet videreudviklet til vindmølleparker i komplekse terræn.
- Jingbian vindmøllepark i komplekse terræn er optimeret med de nye værktøjer med en stigning på 1,46% i AEP.
- Forbedringer i modelleringsværktøjerne WindPRO og WAsP har vist at give bedre forudsigelser end den gamle version WAsP (>10%) og anden, nogle eksisterende CFD kommerciel software (>3%).
- Optimeringsværktøjer er integreret i WindPRO og WAsP, og en ny version er klar til udgivelse.

1.3 Executive summary

A major goal for the project has been to develop new wind farm optimization tools for optimally placing wind turbines in wind farms located in complex terrain supported by full scale measurements in wind farms. The tools will allow EMD International A/S and the Department of Wind Energy, Technical University of Denmark (DTU Wind Energy) to incorporate the created models in their respective software tools (WAsP and WindPRO) as well as to develop consultancy services based on the created modeling tools. The project involves the Sino-Danish collaboration between the Danish partners (DTU Wind Energy and EMD) and the Chinese partners (North-West Investigation and Design Institute and HoHai University) on developing new wind technology. The design of wind farms in complex terrain requires the knowledge of wind resource prediction, wake modeling, ground effects and optimization algorithms and tools. The project is divided into eight work packages (WPs): (1) consortium management, (2) full scale measurements of wind farms in complex terrain, (3) development of complex terrain model, (4) detailed wind turbine wake models, (5) simplified wind turbine wake models, (6) wind farm layout optimization, (7) software evaluation and commercialization, and (8) planning and construction of a new wind farm in complex terrain.

Through the collaboration between Danish and Chinese partners, measurements with 2 metmasts and strain-gauges in a turbine tower were performed successfully in the Chinese Jingbian wind farm with 25 turbines. One-year measurement data and SCADA data have been received. Based on the measurement data, wind farm layout optimization tools have been further developed for wind farms in complex terrain. Furthermore, the optimization tools have been integrated into WindPRO and WAsP and a new version is ready to be released.

1.4 Project objectives

The objective of the project is to develop and provide new reliable tools for designing wind farms located in complex terrain through full scale measurements in wind farms. The models will allow EMD and DTU to incorporate the created models in their respective software tools (WAsP and WindPRO) as well as to develop consultancy services based on the created modeling tools. Specific requirements to the candidate design tools are:

• The (in-house) computational fluid dynamics (CFD) tools should be further validated and improved in cases of wind turbines in complex terrain, especially the turbulence model and the actuator disc model implementations;

• The simplified flow approaches and wake models for wind farm optimization should be further developed for cases with wind turbines in complex terrain;

• The developed wind farm design tools should be verified for wind farms in complex terrain.

The project evolved as foreseen and accordingly to the milestones agreed upon. Measurements were made as planned. Based on the measured data and SCADA data, validations of the existing CFD tools were done as CFD provides reliable base wind resources for wind farm layout optimization. As another essential part of the layout optimization, wake models were further developed to take into account the features from terrain. The final optimization tools were tested for small and large wind farms, and improvements were made as compared to the original wind farms. Finally, the tools were integrated into WindPRO and WAsP and a new version will be released soon.

There are a few risks related to the project. The main risk is related to the measurements. Due to different national rules between Denmark and China, the equipment installation for field measurements was delayed by 1 year. The 1-year delay gave an over-budget for the project as the currency exchange rate went in an unfavorable way.

1.5 Project results and dissemination of results

In this section, the main results from the FarmOpt project are described. It comprises field measurements in China, CFD base flow computation and validation, advanced CFD wake model validation, simple engineering wake model validation and improvement, wind farm layout optimization tool development, software commercialization, and new wind farm development.

1.5.1 Field Measurements in China (WP2)

WP2 contains 2 tasks: Task 2.1: Measurements in a selected wind farm in complex terrain and Task 2.2: Analysis of the measurements data. The objective of the WP is to collect measured data in a wind farm in complex terrain and use the collected data for developing tools for wind farm layout optimization in the subsequent WPs.

Description of the wind farm

The models developed during the project require validation through full scale measurements from a wind farm located in complex terrain. Together with the Chinese partner NWI, DTU Wind Energy obtained access to a wind farm in the northern part of the Chinese Shaanxi region. This wind farm of 50 MW includes 25 large wind turbines, which is located in a complex terrain south of the border to the Inner Mongolia near Jingbian. This wind farm is phase 1 of a larger wind farm and is named Shaanxi wind farm in this description. The inflow to the wind farm is dominated by complex terrain, except for the northern sector, which is rather flat towards the Mongolian plateau. Furthermore, some of the inflow sectors are disturbed by the wakes from nearby single turbines, which were installed after the measurements program was initiated and displayed in Figure 1. One year of wind speed measurements, which were recorded at the site in 2009 before the installation of the wind farm, documents the wind resource and the prevailing wind direction as shown in Figure 2. The annual mean wind speed was 6.27 m/s with prevailing wind directions from the south (S) and north-west (NW).

The wind farm layout is optimized according to the terrain complexity, which has resulted in a height variation between 1 570 and 1 699 m as indicated in Figure 3. The wind turbines are designed and manufactured in China by CSIC, Haizhuang and the main specifications are given in Table 1. The manufacturer's power curve has been used for a verification of the operational behaviour of the turbines, while the thrust coefficient curve has been used for a validation of the tower bending measurements.

Wind turbine #14 is located in the southern part of the wind farm next to a large slope as indicated in Figure 4 and is used for detailed flow analysis. Wind turbine #14 has been equipped with strain gauges for tower bending measurements.

Measurement setup

The measurements consist of three main data systems:

1. SCADA data for each of the 25 wind turbines, provided by the wind farm operator;
2. Wind measurements from two 70m met masts located next to wind turbine #14. The two masts were installed as part of the project;
3. Strain gauge based tower load measurements in the bottom of wind turbine #14 and installed as part of the project.

The planned measurement setup is detailed in (Hansen, 2016) and a sketch of the setup is shown in Figure 5 covering system 2 and 3.

The SCADA data were provided by the wind farm operator as 1-minute statistical mean values for the primary operational signals e.g. active power, pitch angle, rotor speed, yaw position, wind speed on nacelle, and wind direction on the nacelle. These signals, which have been provided for each of the 25 wind turbines, have been qualified and resampled to 10-

minute mean statistics. Furthermore, a calibration of the yaw position signal has been performed. An equivalent rotor wind speed has been derived from the power and pitch values in combination with the power curve. Based on this, each wind turbine can be used to estimate the local inflow conditions in terms of wind speed and wind direction, but only when the turbine is online. All the power values for each turbine are categorized according to the operational status of the turbine, e.g. grid connected, curtailed, start/stop event, idling, stopped or faulty. The validity of the power curves have been controlled for the turbines (#14 and #12) close to the met masts. Unfortunately, it was not possible to validate the operational behaviour of the remaining turbines, except with spot checks of the power curves based on the (biased) nacelle wind speed.

Installation of measurement instruments on two met masts next to wind turbine #14 were performed by Chinese and Danish personnel. The instrumentation includes cup anemometers, wind vanes, 3D-sonic anemometers, thermometers and barometers as shown in Figure 5. A NRG logger was used to record the 10-minute statistical values from the cup anemometers, wind vanes, thermometers and barometers.

The DTU Data Acquisition (DAQWIN) logger with a sampling frequency of 35 Hz was used to record time series from strain gauges installed in the tower, which should be used to estimate the rotor thrust during operation. Furthermore, time series from the power transducer and three 3D sonic anemometers were measured. The sonic time series are used to determine the vertical wind speed and dynamic behaviour of the wind speed together with the atmospheric stability (Monin-Obukhov Length MOL). MOL is used to obtain an onsite classification of the stratification. Due to lack of calibration information it was necessary to calibrate the tower bending moments with use of the estimated thrust times the elevation height. This is not an exact calibration and will only enable a determination of the relative variation of the tower bending and the derived thrust coefficient.

A database of synchronized, qualified measurements including SCADA data, statistical values for the meteorological measurements, and the tower loadings, has been established as part of the measurement project. The database, named SHAANXI, is hosted by DTU Wind Energy and a brief summary of the contents of the database is presented in Table 2. The SCADA data and mast measurements represent a complete year, while the time series only represents a ½ year of measurements. The reduced amount of measurements is due to problems with the logger access at the remote location.

Flow analysis

The flow analysis has been focusing on the definition of model validation cases. As mentioned previously, the inflow conditions for each wind turbine has already been determined, but a detailed analysis revealed that some of the turbines in a neighbouring wind farm caused some sector-wise inflow disturbances to the wind farm. The reference turbines #11 and #14, with undisturbed inflow, was used in the definition of flow cases for benchmarking the flow models.

The mean power for each wind turbine has been averaged for an inflow sector using a moving window of 10 degrees in the range 0 - 360 degrees for wind speed interval of 3-5 m/s. The results are presented in Figure 6 and the figure demonstrates a large variability for the power values. The power ratio = Pmax/Pmin of the 10-minute power values varies from 2 to 9. The variability is caused by a combination of the terrain effects, wake effects and the operational behaviour of the turbines. The flow cases used for validation are defined in Table 3. The wake deficit between pairs of turbines as shown in Figure 7 for westerly inflow has been analysed and demonstrates a decreasing peak deficit for increasing spacing. The corresponding peak power deficit values are listed in Table 4.

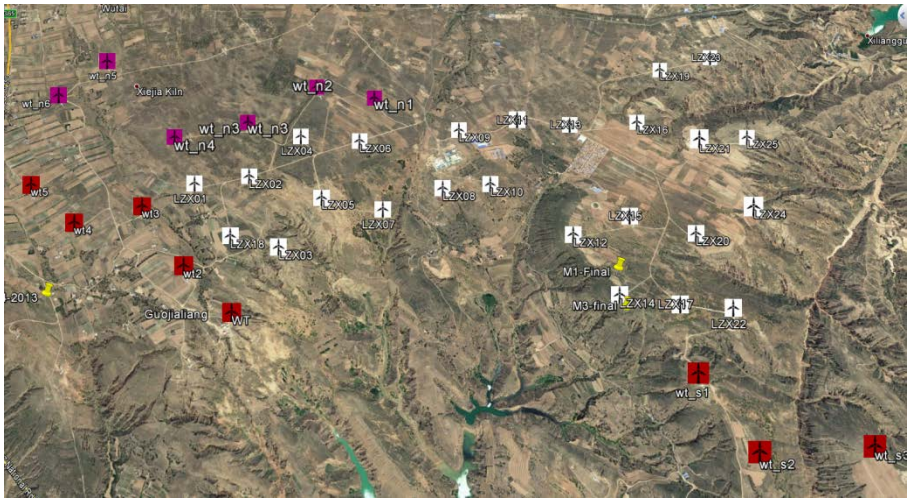

Figure 1: Shaanxi windfarm marked with white labels together with nearby "disturbing" wind turbines installed during a later phase, where the map has been downloaded from the Google Earth server.

Detailed flow analysis around wind turbine #14 based on recordings from the two masts present the distinct wind speed deficit and the increased turbulence behind the turbines #12 & #14 for the inflow from northwest-north (NW-N) sector.

Analysis of the DEL values for the tower bending in the fore-aft direction demonstrates an increased fatigue loading for westerly inflow perpendicular to the slope compared to flat, uniform inflow for sector N.

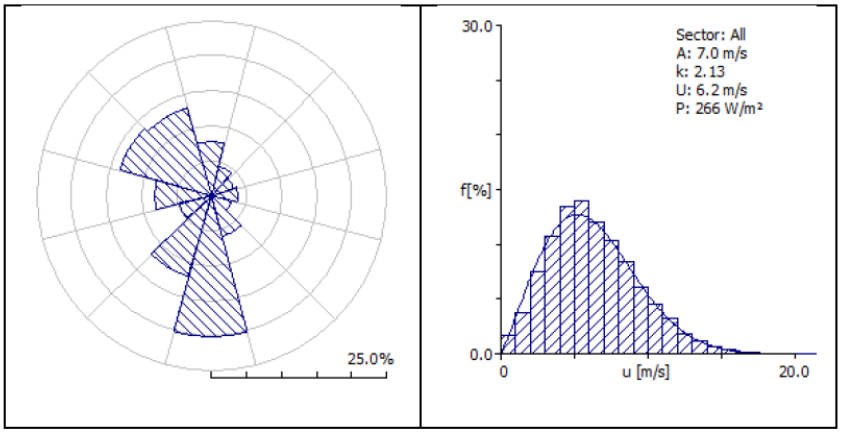

Figure 2: Wind climate at the wind farm measured during 2009 at 70m height. The climate measurements have been recorded in the northern part of the wind farm next to WT#13 before the wind farm installation.

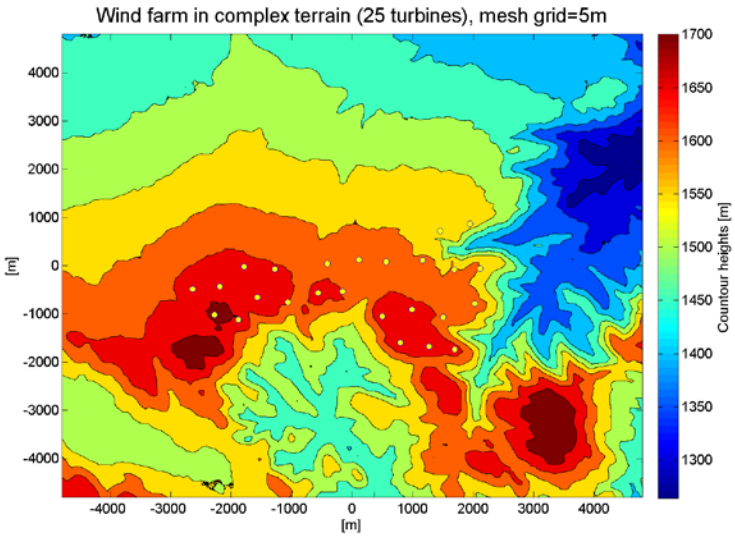

Figure 3: Wind farm landscape contour plot including location of 25 wind turbines (the white circles represent the wind turbines).

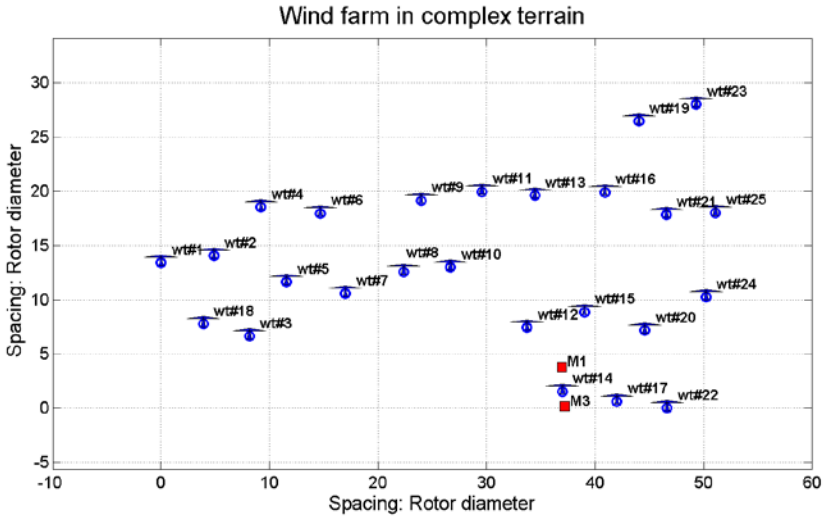

Figure 4: Layout for the Shaanxi wind farm in complex terrain, where the unit is equal to the rotor diameter of 93 m. Two met masts are installed next to turbine wt#14, which is located on top of an escarpment. M1 is located approximately at the level of the wt#14, while M3 is located approximately 17 m below wt#14 on the slope.

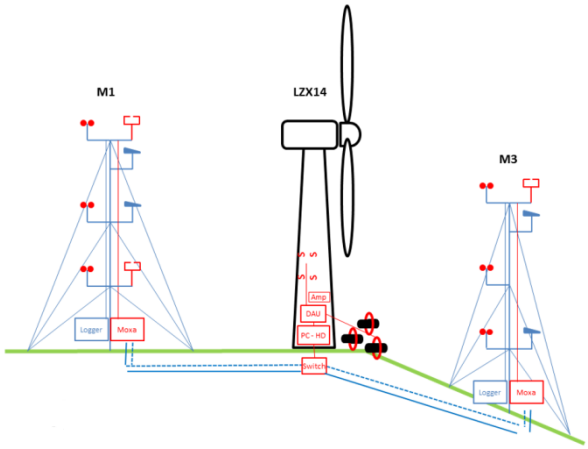

Figure 5: Measurement setup for 2 met masts and wind turbine #14.

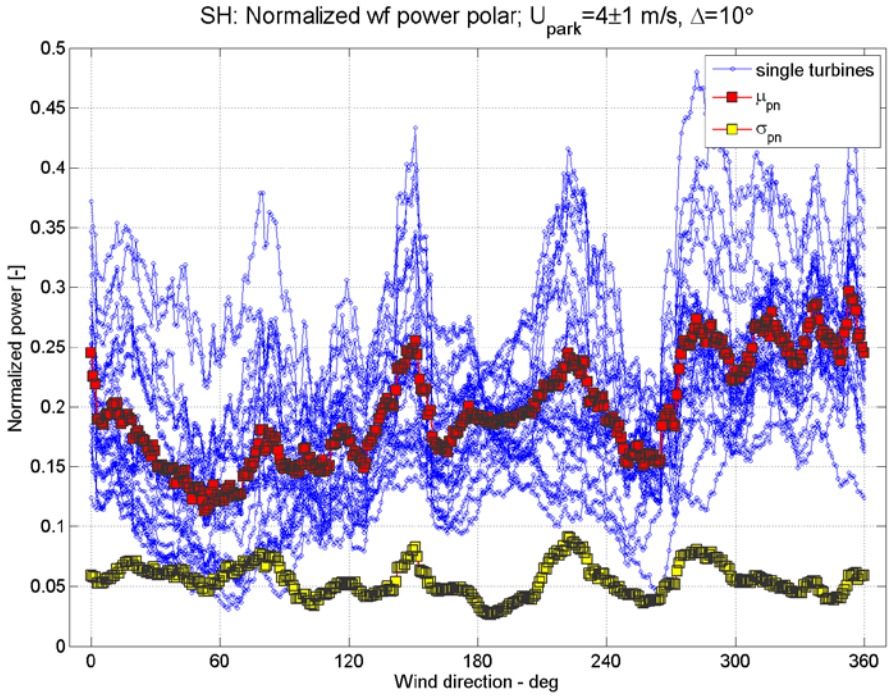

Figure 6: Normalized sector-wise mean power for each wind turbine in the wind farm. Furthermore, the figure includes the normalized and average park power production (μPN) and standard deviation (σPN).

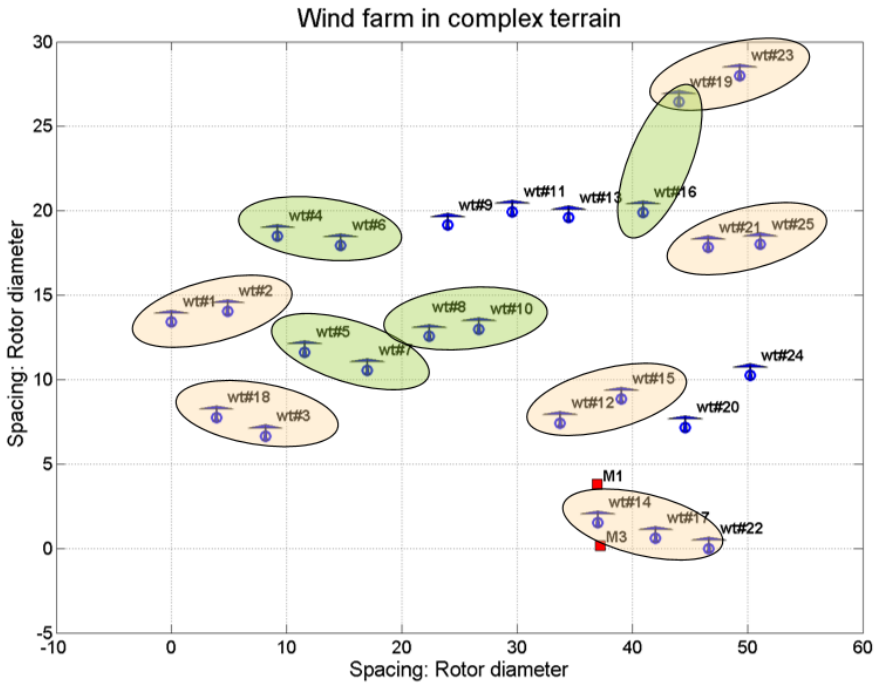

Figure 7: Power deficit distributions between pairs of turbines, with 4, 5, 6 or 7D spacing.

Table 1: Wind turbine specifications.

	Wind turbine 25 x Model 1	Wind turbine 1 x Model 2
Name	CSIC H93-2.0MW	E-82
Diameter	93 m	82 m
Power	2.0 MW	2.0 MW
Hub height	67 m	78 m
Power control	Variable speed, single blade pitch control	Gearless variable speed, single blade pitch control

Table 2: Summary of measurements stored in the database.

hours	Mast M1	Mast M3
speeds, 10-minute	8760	8915
Temps, 10-minute	8450	8720
Wind dir., 10-minute	8470	8700
SCADA data - hours	Min	Max
Power, gross	8100	9000
Power, net	3200	5900
speeds derived	3960	6360
Time series	Hours	
Sonics	4440	
Tower bending	4480	
Thrust, derived	4480	
Active power	N/A	

Table 3: Definition of flow cases for benchmarking flow models with reference to the wind farm flow analysis in the Shaanxi wind farm.

FC	Sector	Wind speed, h=67 m	Reference Wind speed	Reference Wind direction
1.1	180±5°	4±1 m/s	WT14, h=67m	M3, h=60m
1.2	300±5°	4±1 m/s	WT11, h=67m	M1, h=60m
1.3	330±5°	4±1 m/s	WT11, h=67m	M1, h=60m
1.4	180±5°	7±1 m/s	WT14, h=67m	M3, h=60m
1.5	300±5°	7±1 m/s	WT11, h=67m	M1, h=60m
1.6	330±5°	7±1 m/s	WT11, h=67m	M1, h=60m
1.7	180±5°	10±1 m/s	WT14, h=67m	M3, h=60m
1.8	300±5°	10±1 m/s	WT11, h=67m	M1, h=60m
1.9	330±5°	10±1 m/s	WT11, h=67m	M1, h=60m

Table 4: Peak values for the power deficit.

spacingD	wt1#	wt2#	WD deg	Peak %	Width deg	Slope
4	8	10	260	47.8	20	-4%
4	18	3	273	22.7	16	8%
5	14	22	277	43.5	24	-3%
5	11	13	269	41.1	27	-3%
5	12	15	253	34.7	24	-6%
5	4	6	260	29.7	30	14%
5	1	2	257	27.9	26	8%
5	21	25	260	22.6	24	-1%
5	14	17	280	16.4	16	-5%
6	5	7	271	55.7	20	11%
6	18	2	170	43.4	24	-19%
6	3	5	221	33.6	20	23%
6	16	21	290	27.6	40	-11%
6	15	20	277	21.9	20	-4%
6	2	4	229	19.4	25	6%
6	7	8	245	17.1	20	-2%
6	19	23	250	13.7	16	-3%
6	20	24	245	4.7	16	-3%
7	16	19	199	40.6	20	0%
7	10	9	156	35.3	24	-2%
7	12	14	329	34.6	20	-5%
7	2	5	279	34.2	24	22%
7	17	20	197	33.1	20	-2%

1.5.2 Development of a complex terrain CFD model (WP3)

WP3 consisted of two tasks: T3.1 “steady and unsteady CFD simulations and validation” and T3.2 “Development of simple, complex terrain models”. T3.1 dealt with development and validation of CFD models that can accurately calculate the flow in complex terrain, i.e. forested sites and terrain with steep slopes; while task T3.2 aimed to implement the developed CFD models into a simple-to-use software that is usable as part of the wind farm layout optimisation. Below is a review of the publications made as part of the development and validation of the CFD model (T3.1). Section 1.5.6 describes the integration of the CFD model with the commercial software WasP-CFD and WindPRO (T3.2).

Four main publications have been made to develop and validate the CFD model for complex terrain. Each publication investigates a topic necessary to ensure an accurate CFD model usable for wind farm layout optimisation. The sections below give a summary of each publication.

CFD for wind resource assessment in steep terrain (*Troen and Hansen, 2015*)

(Troen and Hansen, 2015) uses the wind atlas methodology to predict the mean wind speed at nine complex sites with a total of 26 mast locations. The purpose of the study is to compare the prediction “skill” of the traditional IBZ flow model built into WAsP with the ElipSys3D CFD model. Apart from the two flow models, the simulations are conducted using identical maps, wind data and site specifications. The study therefore directly investigates the importance of the flow model for wind resource assessment in complex terrain. The paper finds that the CFD model can provide small but significant improvements relative to the IBZ model.

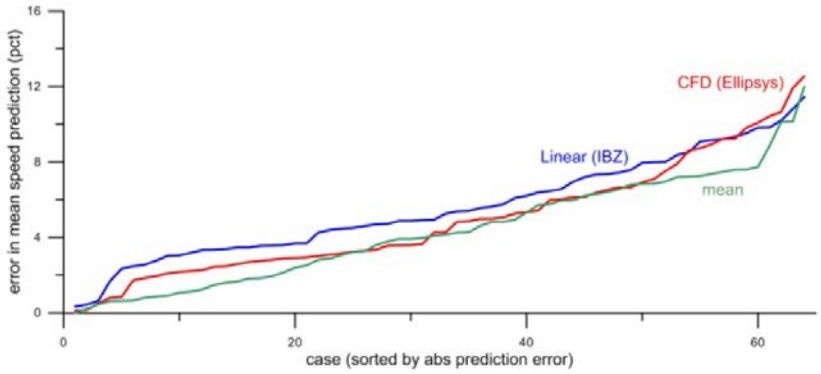

Figure 8: Relative mean speed prediction errors. Blue is std. WAsP, The red curve shows CFD performance. (Troen and Hansen, 2015)

CFD for turbulence assessment in forests (*Sogachev et al., 2015*)

(Sogachev et al., 2015) models the flow over the forested area of Østerild using the two CFD models SCADIS and EllipSys3D. Even though the two models use different two-equation RANS closures, the model approach adapts an extra-diffusion term that ensures consistency between the two models. The CFD results compare well with measured values of turbulence intensity inside the forest and are readily applicable to any two-equation RANS CFD model.

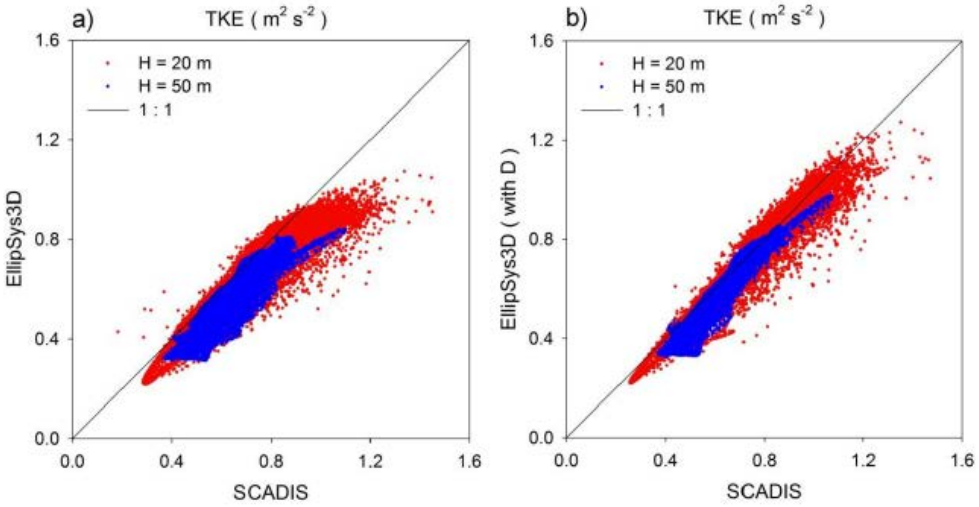

Figure 9: Comparison of modelled values of turbulent kinetic energy of the SCADIS and EllipSys3D CFD models at 20 m (red) and 50 m (blue) AGL. Results are comparable when the extra-diffusion term is included (right). (Sogachev et al. 2015)

CFD turbulence for load assessment (*Svenningsen et al., 2016*)

(Svenningsen et al., 2016) assesses the accuracy of using modelled ambient turbulence for calculation of wind turbine fatigue loads. Results of the WAsP Engineering and the WasP CFD models across 23 non-complex sites compare very well with measurements. Therefore, modelled ambient turbulence from CFD can be used for estimation of wind turbine fatigue loads and be part of a wind farm layout optimisation.

CFD grid resolution (*Bechmann, 2016*)

(Bechmann, 2016) investigates the requirements of CFD models to minimise numerical errors. The study focuses particularly on the requirements for the resolution of the CFD grid, and the discretisation scheme used in the convective term of the RANS equations. The report concludes that a fine resolution (<=20 m) and a high order discretisation scheme (3rd order Quick) is needed to achieve the accuracy needed for wind resource assessment.

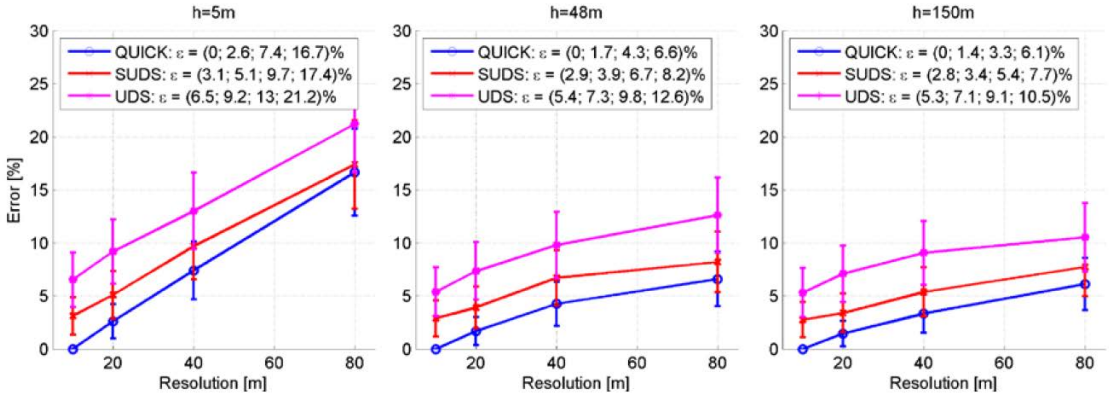

Figure 10: Mean absolute wind speed error as a function of CFD grid resolution in the target area for 5 m (left), 48 m (middle) and 150 m (right) above ground. The colours represent different discretisation schemes: QUICK (blue), SUDS (red) and UDS (pink). (Bechmann, 2016)

1.5.3 Advanced CFD wake modelling (WP4)

In WP4, advanced wake modelling tools are validated against measurements in WP2, which include the actuator disc-Reynolds averaged Navier-Stokes (AD-RANS) model, and Actuator Line-Large Eddy Simulation (AL-LES) model. The validations of the AD-RANS model under atmospheric stability conditions are also performed.

Wind farm simulations using AD-RANS approach in neutral conditions

In this section, the results from the actuator disc-Reynolds averaged Navier-Stokes (AD-RANS) simulations of the Jingbian, Shaanxi wind farm are described. This section contains a brief description of the methodology, results from the simulations, and conclusions.

The wind farm is simulated using computational fluid dynamics (CFD) software developed in-house at DTU Wind Energy. The CFD software used in the present work is called EllipSys3D. To simulate the Shaanxi wind farm, the inputs to EllipSys3D consists of the number of wind turbines, the wind turbine properties such as size and power rating, the location of each turbine in the farm, the terrain topography of Shaanxi, and parameters describing the wind flow in the farm. There are few unique methodologies available in EllipSys3D for simulating different kinds of problems. The AD-RANS approach is one methodology that is suitable for simulating wind farms and is used here for the farm in Shaanxi.

Based on twelve months of met mast and turbine measurements, nine plus eight (seventeen in total) wind farm flow cases have been identified for validating the AD-RANS simulations. The flow cases are divided into two groups: FC1 and FC1p, as shown in Tables 5 and 6, respectively, below. Only the results from FC1 will be provided in this report for brevity.

Table 5: Inflow conditions for flow case FC1 where h=height and WT=wind turbine.

FC	Sector	Wind speed, h=67 m	Reference Wind speed	Reference Wind direction
1.1	180±5°	4±1 m/s	WT14, h=67m	M3, h=60m
1.2	300±5°	4±1 m/s	WT11, h=67m	M1, h=60m
1.3	330±5°	4±1 m/s	WT11, h=67m	M1, h=60m
1.4	180±5°	7±1 m/s	WT14, h=67m	M3, h=60m
1.5	300±5°	7±1 m/s	WT11, h=67m	M1, h=60m
1.6	330±5°	7±1 m/s	WT11, h=67m	M1, h=60m
1.7	180±5°	10±1 m/s	WT14, h=67m	M3, h=60m
1.8	300±5°	10±1 m/s	WT11, h=67m	M1, h=60m
1.9	330±5°	10±1 m/s	WT11, h=67m	M1, h=60m

Table 6: Inflow conditions for flow case FC1p where h=height and WT=wind turbine.

FC	Sector	Wind speed, h=67 m	Reference Wind speed	Reference Wind direction
1p.1	60±5°	4±1 m/s	WT11, h=67m	M1, h=60m
1p.2	100±5°	4±1 m/s	WT25, h=67m	M1, h=60m
1p.3	240±5°	4±1 m/s	WT14, h=67m	M1, h=60m
1p.4	360±5°	4±1 m/s	WT11, h=67m	M1, h=60m
1p.5	60±5°	7±1 m/s	WT11, h=67m	M1, h=60m
1p.6	100±5°	7±1 m/s	WT25, h=67m	M1, h=60m
1p.7	240±5°	7±1 m/s	WT14, h=67m	M1, h=60m
1p.8	360±5°	7±1 m/s	WT11, h=67m	M1, h=60m

Figures 11 to 19 contain the AD-RANS results and the comparisons with the measurement data from a data acquisition (SCADA) system. The figures contain the predicted (labelled as AD Avg and AD Exact) and measured (labelled as SCADA) electrical power output for all 25 wind turbines. Each wind turbine is labelled between 1 and 25. Figures 11 to 19 contain the results for the FC1 flow case. Results for the FC1p flow case are not shown for brevity. The notation “wd” and “ws” shown in the title for each figure denotes “wind direction” and “wind speed”, respectively. The wind direction corresponds to the measurements on met masts “M1” and “M3”, while the wind speed corresponds to the measurements on the reference wind turbine (WT). The SCADA measurements represent averaged values in +/- 5-degree bins. The AD Exact results represent a single run equal to the wind direction specified in the figure title. The AD Avg results represent the average of five runs: -5, -2, 0, +2, and +5 degrees relative to wd. For example, AD Exact in Figure 11 is a single run at 180 degrees, and AD Avg is the average of 5 runs: 180 – 5, 180 – 2, 180, 180 + 2, and 180 + 5 degrees.

FC1:

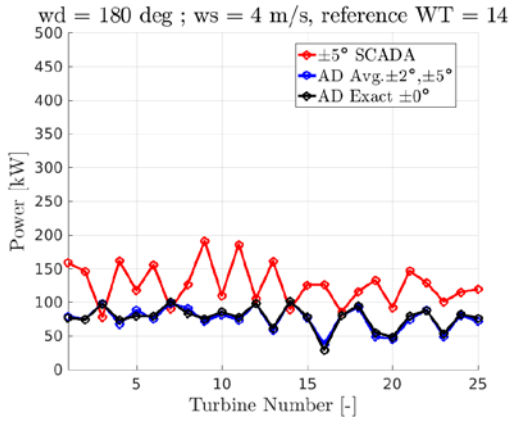

Figure 11

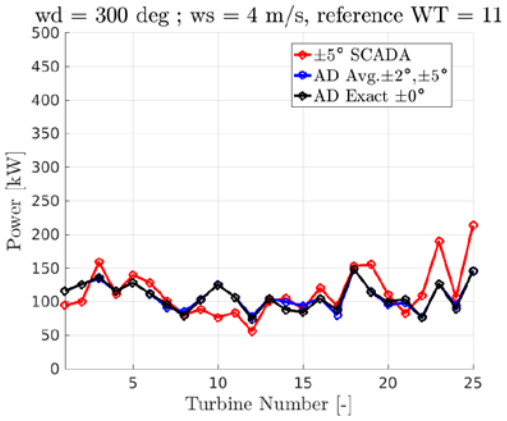

Figure 12

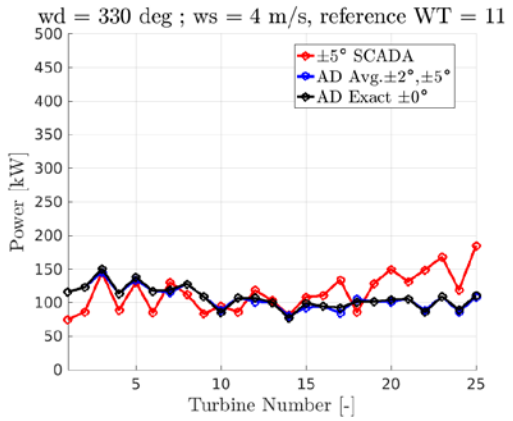

Figure 13

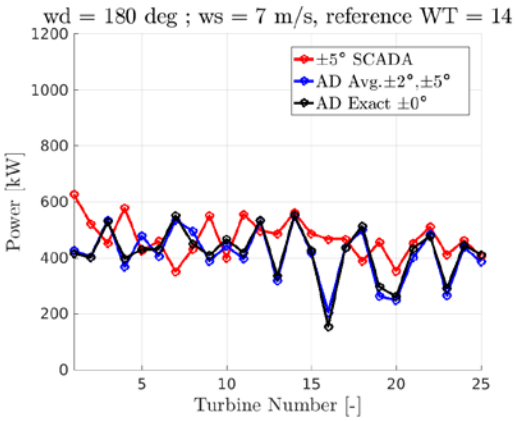

Figure 14

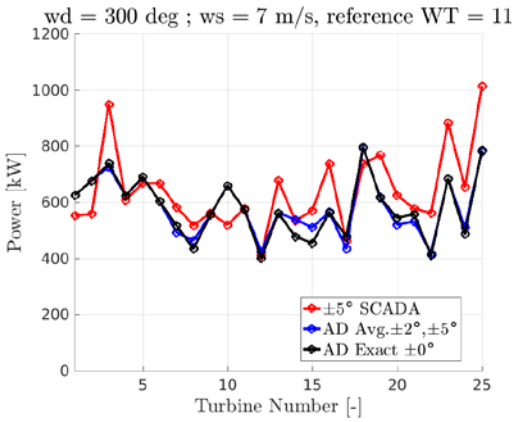

Figure 15

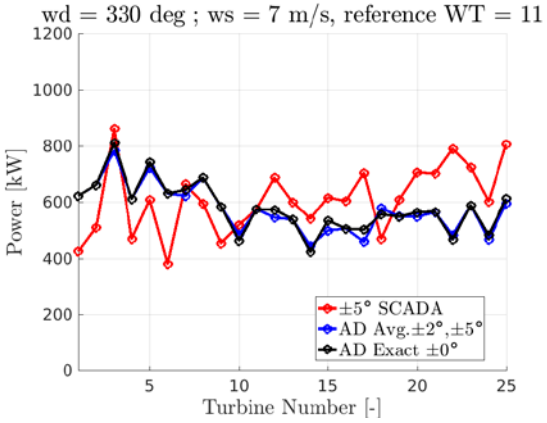

Figure 16

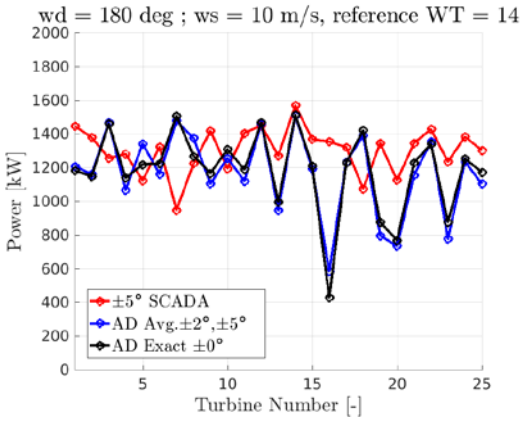

Figure 17

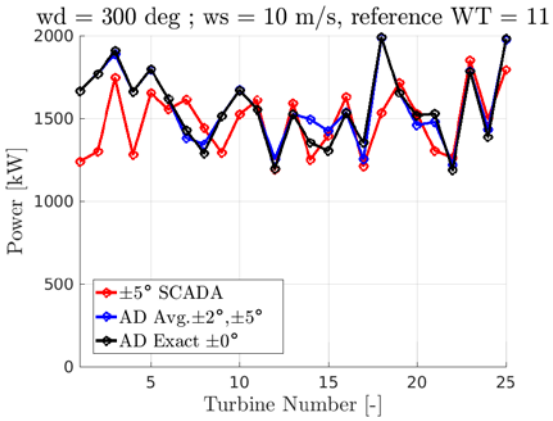

Figure 18

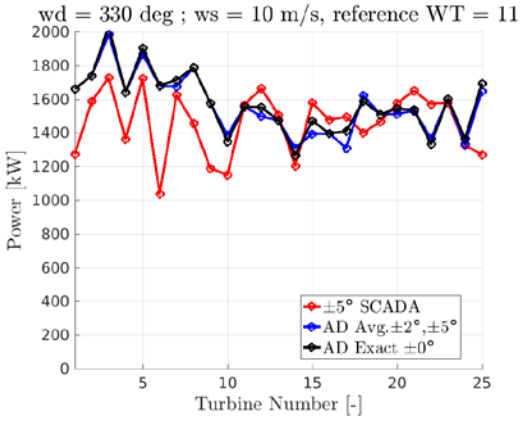

Figure 19

In Figures 11 to 19, AD Avg should more closely represent the SCADA measurements than AD Exact, since the SCADA measurements are grouped and averaged in +/- 5-degree bins. The SCADA results cannot be determined exactly at 180 degrees in Figure 11, for example. Nevertheless, the AD-RANS results in Figure
s 11 to 19 show that AD Avg is almost identical to AD Exact. Considering that the measurements likely include many physical phenomena that cannot be captured in a computer simulation (e.g. wake to wake interactions, turbulence, etc.) and possibly many other unknown effects, both AD Exact and AD Avg are in reasonable agreement with measurement values.

Detailed simulations of wind turbine number 14 using LES in neutral conditions

In this section, the results from the actuator line, large eddy simulation (AL-LES) of wind turbine 14 in the Jingbian, Shaanxi wind farm are described. This section contains a brief description of the methodology, results from the simulations, and conclusions.

In addition to AD-RANS, EllipSys3D can perform AL-LES computations. AL-LES provides much more detailed information about the wind flow than AD-RANS, but at the expense of a much higher computational cost. Therefore, in contrast to the AD-RANS simulations of the entire Shaanxi wind farm described above, the AL-LES is applied to a much smaller area,

specifically around wind turbine 14. The smaller area contains wind turbine 14 and the two met masts M1 and M3. The area around wind turbine 14 is selected specifically because it is near two met masts and the results from the simulations can be compared with measurements from the met masts. The inputs to AL-LES are almost identical to the AD-RANS.

Due to the large computational expense of the AL-LES simulations, only four cases are considered: 4 and 7 meters per second from south to north (wd=180 degrees) and north to south (wd=0 or 360 degrees). These four cases were selected based on the measurements at the site, which showed that the wind in the Shaanxi wind farm in the south-north direction was the most frequent and contained more reliable measurement data. Figure 20 depicts an AL-LES simulation of wind turbine number 14 at 7 m/s wind speed from south to north. The comparison of AL-LES results with measurement data are shown in Table 6 and Figures 21 to 23.

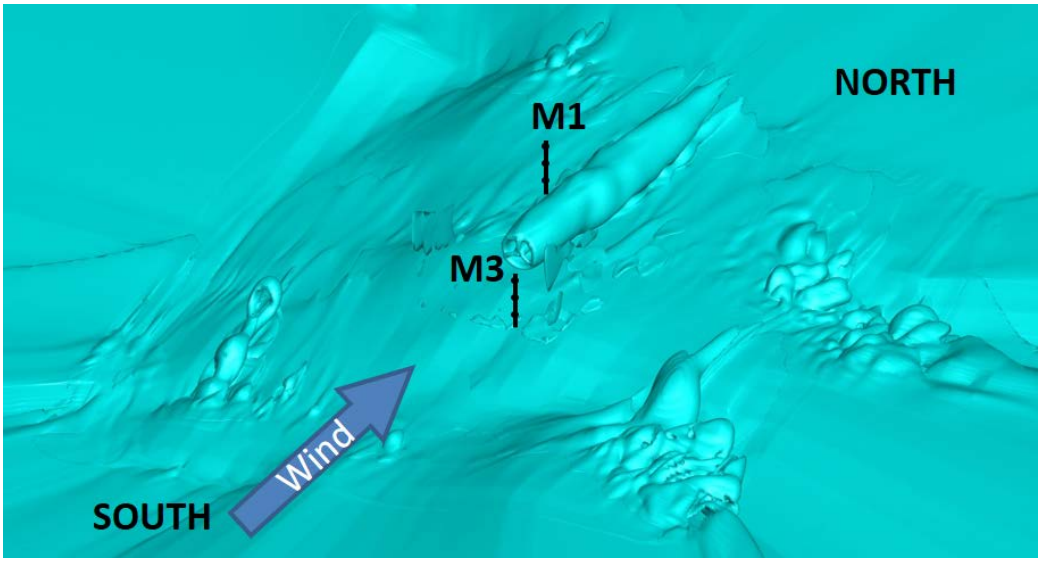

Figure 20: Actuator line (AL), large eddy simulation (LES) of wind turbine number 14 at 7 m/s wind speed from south to north. M1 and M3 are met masts.

In Table 6, the mean power (kW), generator speed (RPM), and wind speed at 30, 50, and 70-meter heights on met masts M1 and M3 for the four flow cases are shown. The table includes the results from the AL-LES in black, the averaged measurement values in blue, and the percent difference between the AL-LES and the measurements in green. There is reasonable agreement between the AL-LES and the measurements for the power and generator speed on wind turbine 14, the largest percent difference being 13.12% in power for the 0°, 7 m/s flow case. Larger percent differences were obtained for the wind speeds, particularly when comparing AL-LES and the measurements for the met mast located downstream of wind turbine 14. For example, the percent difference in wind speed at 70 m height on met mast M1 for the 180°, 4 m/s flow case is 28.81%. The reason for the large difference is because M1 is located downstream of wind turbine 14 as shown in Figure 20. The complexity and stochastic nature of the turbulence from the wake of wind turbine 14 introduces larger variations and uncertainty in the flow field.

Table 6: Summary of AL-LES results (black), measurement values (blue) and percent difference between the simulation and measurements (green).

SCADA in Blue % Diff. in Green	180°, 4 m/s	180°, 7 m/s	0°, 4 m/s	0°, 7 m/s
Power (kW)	142 156.6 -9.32%	714.3 709.0 0.75%	123.1 117.8 4.50%	774.99 685.1 13.12%
Generator speed (RPM)	886.0 886.8 -0.08%	1472.0 1468.0 0.27%	886.0 894.0 -0.89%	1452.0 1464.6 -0.86%
Windspeed (m/s) @ 70 m **M3**	4.149 4.143 0.15%	7.027 7.036 -0.12%	1.560 2.263 -31.06%	3.066 3.862 -20.61%
Windspeed (m/s) @ 50 m **M3**	3.891 3.867 0.62%	6.590 6.669 -1.19%	2.308 2.025 13.98%	4.302 3.643 18.10%
Windspeed (m/s) @ 30 m **M3**	3.547 3.719 -4.62%	6.009 6.294 -4.54%	3.217 2.464 30.57%	4.845 5.143 -5.80%
Windspeed (m/s) @ 70 m **M1**	1.902 2.671 -28.81%	3.294 3.707 -11.13%	4.068 4.05 0.46%	7.155 7.114 0.58%
Windspeed (m/s) @ 50 m **M1**	2.554 2.614 -2.30%	4.457 3.933 13.30%	3.741 3.888 -3.76%	6.582 6.814 -3.42%
Windspeed (m/s) @ 30 m **M1**	3.554 3.090 15.01%	6.042 5.104 18.38%	3.306 3.588 -7.85%	5.818 6.343 -8.28%

Figures 21 to 23 are the results in Table 6 displayed in a bar-chart format. The results for the wind speed comparisons are grouped as upstream (Figure 22) or downstream (Figure 23). In Figure 21, the largest difference between the AL-LES (Simulation) and measurements (Measured) appears for the power in the 0°, 7 m/s flow case. All other comparisons in Figure 21 are in good agreement. Figure 22 shows that the comparisons for wind speed for the upstream mast are in better agreement than the comparisons for the downstream mast shown in Figure 23. As mentioned previously for Table 6, larger differences occur for the downstream mast because of the complexity and stochastic nature of the turbulence generated from the wake of wind turbine 14. The wake of wind turbine 14 introduces larger variations and uncertainty in the flow field.

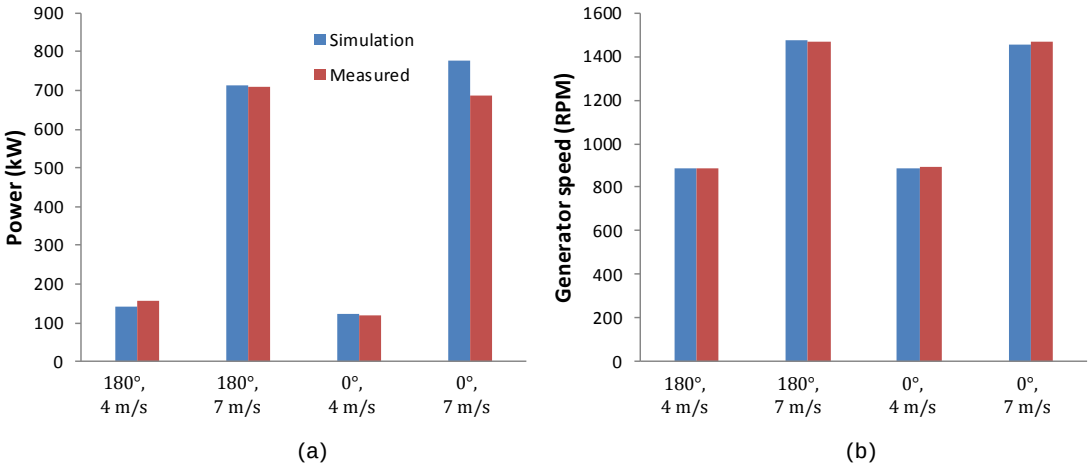

Figure 21: Comparison of AL-LES (simulation) and measured (a) power and (b) generator speed of wind turbine 14 for the four flow cases.

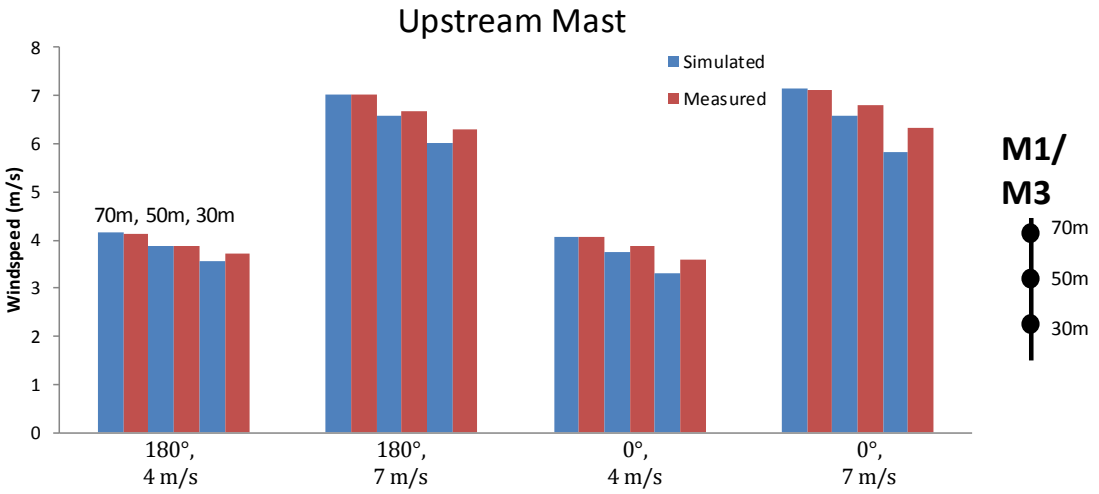

Figure 22: Comparison of AL-LES (simulated) and measured wind speeds at 30-, 50- and 70-meter heights on masts M1 and M3 when M1 and M3 are upstream of wind turbine 14.

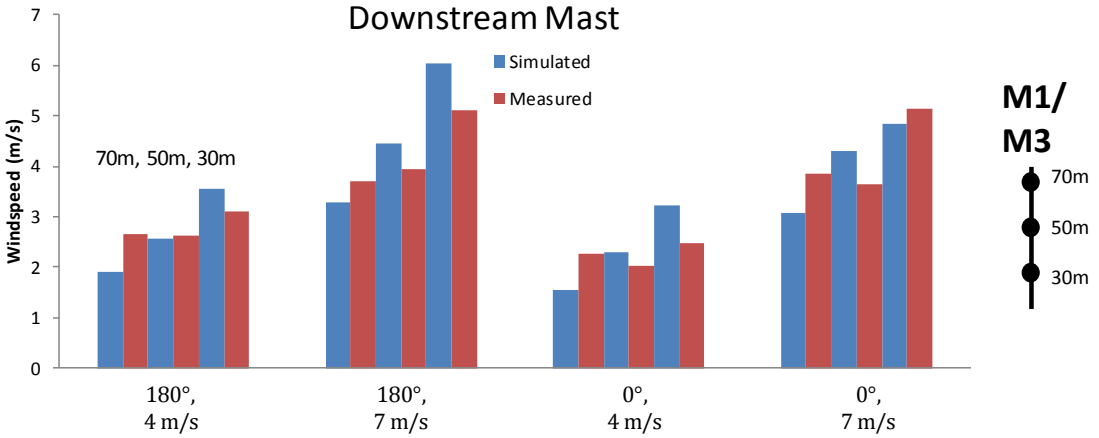

Figure 23: Comparison of AL-LES (simulated) and measured wind speeds at 30-, 50- and 70-meter heights on masts M1 and M3 when M1 and M3 are downstream of wind turbine 14.

Wind farm simulations using AD-RANS approach including the effect of stability

In this section, the results from the actuator disc, Reynolds-Averaged Navier Stokes (AD-RANS) simulations of the Jingbian, Shaanxi wind farm for neutral and stable atmospheric conditions are described. Wind farm energy production and lifetime are strongly influenced by the characteristics of the atmospheric boundary layer (ABL). Therefore, it is important to investigate the ABL in unstable, neutral and stable conditions. This section contains a brief description of the methodology, results from the simulations, and conclusions.

As already mentioned above, the wind farm is simulated using CFD software called EllipSys3D developed at DTU Wind Energy. To simulate the Shaanxi wind farm in non-neutral (i.e. unstable or stable) conditions, additional inputs to those described above are required. The additional inputs are associated with a simple model based on Monin-Obukhov similarity theory (MOST) to simulate the effect of atmospheric stability. Based on twelve months of met mast and turbine measurements, only three wind farm flow cases are used for comparing the AD-RANS simulations with measurement data in neutral and stable atmospheric conditions. Difficulties were encountered with AD-RANS simulations for unstable conditions and are not included in the present report.

Figures 24 to 26 contain the AD-RANS predictions of electrical power output for all 25 wind turbines in neutral and stable conditions. In Figures 24 to 26, the predictions in neutral and stable conditions are labelled as Neutral and Stable, respectively. The measurement data from the data acquisition system for neutral and stable conditions are labelled as Neutral

SCADA and Stable SCADA, respectively. Identical to the neutral cases, the notation “wd” and “ws” shown in the title for each figure denotes “wind direction” and “wind speed”, respectively. The wind speed, *ws*, corresponds to the measurements on the reference wind turbine WT=14. The SCADA measurements represent averaged values in +/- 5-degree bins. The AD RANS results represent a single run equal to the wind direction specified in the figure title. Averaged AD-RANS results between five runs: -5, -2, 0, +2, and +5 degrees, are not included here for brevity.

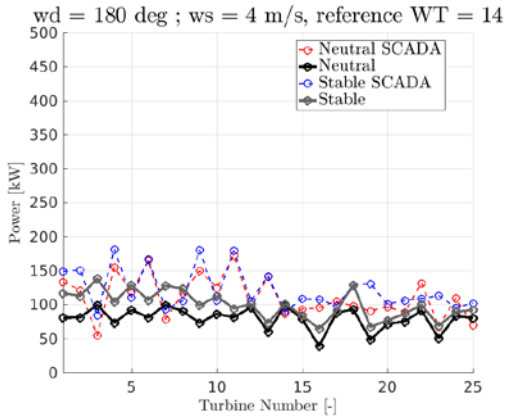

Figure 24

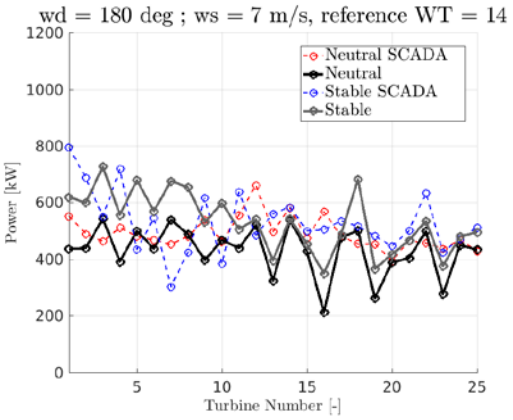

Figure 25

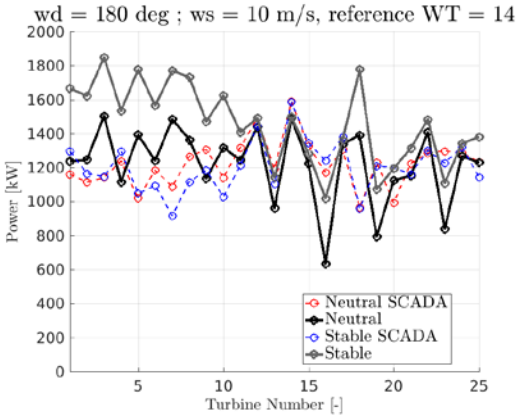

Figure 26

In Figures 24 to 26, the neutral AD-RANS results are nearly identical to those shown in Figures 11 to 19, as expected. The stable AD-RANS results, however, show an increase in electrical power output compared to the neutral case. The increase in electrical power output is due to the higher wind speed occurring around hub height in the stable scenario. The higher wind speeds at hub height for stable conditions are consistent with findings found in the literature. A slight increase in electrical power output from neutral to stable is also seen in the SCADA values, but it is not as significant as in the AD-RANS simulations. For higher wind speeds, i.e. ws=10 m/s in Figure 26, the stable AD-RANS results over-predict the electrical power output, particularly for wind turbine numbers 1 to 10. The MOST implementation in the AD-RANS requires further development, since it is only accurate up to 100 m heights, does not include the effect of buoyancy forces, and is missing other physical phenomena captured in the SCADA.

1.5.4 Engineering wake modelling (WP5)

WP5 contains 2 tasks: 1) Development of fast simplified wake models (Jensen wake model, Fuga model and Dynamic Wake Meandering (DWM) model), and 2) linking simplified wake models to detailed RANS CFD terrain models.

Ambient flow fields in moderately complex terrain

Undulating terrain modifies the wind field. A relatively shallow hill will have a similar effect as an airfoil with increased velocity (speed-up) at the summit. The speed-up driven by a pressure drop at the hilltop that accelerates the flow and brings streamlines closer to the ground. For steep hills the flow lines detach from the ground, and a *recirculation zone* develops on

the lee side of the hill. This is analogous to stall on an airfoil when the angle of attack exceeds a certain limit. For wind blowing perpendicular to a Gaussian ridge recirculation occurs when the maximum slope angle exceeds about 17 degrees. 17 degree corresponds to a slope of *tan* 17^o=30%, which is actually quite steep. Roads would for example require hairpin bends to function. Recirculation zones are *not* necessarily stationary, but may come and go switching randomly between attached and detached flow. Only a time resolved model (i.e. CFD DNS or LES) can deal with such toggling behavior, but such computational approaches has already been excluded as irrelevant for practical WF design purposes (cf. section Introduction).

For ordinary RANS the relevance of the Reynolds decomposition is questionable, because the mean flow does *not* represent any of the two alternating flow patterns, so that predictions of the flow inside recirculation zones are quite uncertain. In any case, operating wind turbines inside recirculation zones does not seem to be a good idea, and most wind farms are placed in terrain sufficiently shallow to preclude the generation of recirculation zones. We will refer to this as *moderately complex terrain*, and limit rest of this study to such types of terrains. The 2D ridge-type of terrain is, compared more 3D like types of terrain complexities, considered the most critical for flow recirculation, as complexities with more 3D-like characteristics will, popular speaking, offer the flow more possibilities to 'escape' without forming detached flow regimes. We will, therefore, conservatively retain the 17 degree limitation for complex terrains in general.

Fast computation of streamlines and speed-up using a generalized Fuga model

Conventional CFD RANS computations can be quite CPU-demanding when it comes to simulation of streamlines and speed-up effects under complex terrain topologies. Therefore, an extremely fast linearized RANS model has been developed for this purpose. The model is basically the 'classic' Fuga model - which has proven a very efficient tool for flat and homogeneous terrain conditions - generalized to moderately complex terrain conditions.

When there are no recirculation zones, the mean flow streamlines extend from infinitely far upwind to infinitely far downwind. It is therefore possible to define new coordinates (x', y', z') for the 'classic' Fuga model in such a way that y' and z' are constant along (mean flow) streamlines, which therefore run in parallel with the x'-axis. This property is not spoiled if x' is redefined, and we can therefore choose x' so as to make the coordinate transformation *volume preserving*. The new coordinates are *terrain following* and the flow domain extend from $z' = 0$ to some maximum value at the lid, and the velocity vanishes at $z' = z_0$. In other words, the boundary conditions are the same as for flow in homogeneous terrain and contain no reference to the terrain. This information appears now in the Jacobian matrix of the transformation

$$J_{ij} = \frac{\partial x_i'}{\partial x_j} \tag{1}$$

which pops up in the governing equations when derivatives are expressed in terms of the new coordinates. For an incompressible flow there are two such equations: the continuity equation and the momentum equation (for the three velocity components), which we will take as RANS with an eddy viscosity. The math is quite complicated - the details can be found in (Larsen, 2018).

An example of computed streamlines in a real complex terrain is shown in Figure 27.

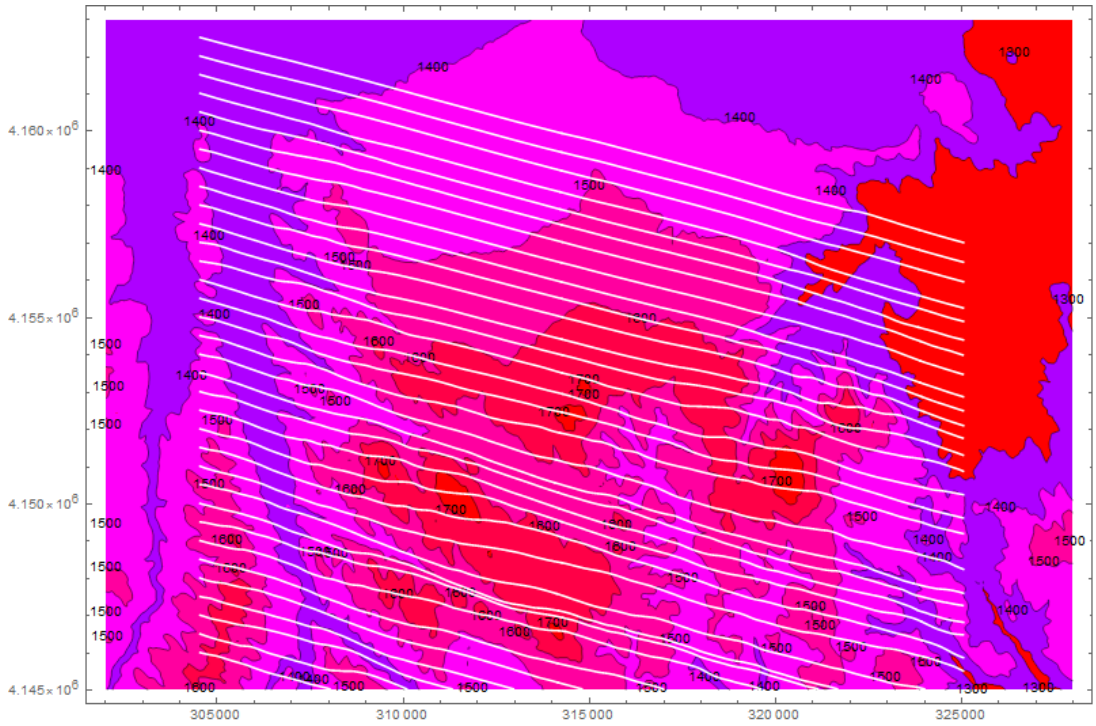

Figure 27: Computed streamlines in complex terrain conditions.

A comparison was also made with Paul van der Laan's RANS k-ε-f_P model. The terrain is a Gaussian hill:

$$h(x,y) = H\, e^{-\frac{x^2+y^2}{2\,\sigma^2}}$$

where $H = 126$ m and $\sigma = 250$ m corresponding to a maximum terrain inclination of 17 degrees. The surface roughness was set to 3 cm. Two RANS calculations were made for each of the following 8 cases: one with an actuator disk of diameter D and one without. The position of the actuator disk is found as follows:

Case 1:	$D = H,\quad X_{AD} = 0,\quad Y_{AD} = 0,\quad Z_{AD} = D$
Case 2:	$D = H,\quad X_{AD} = -5H,\quad Y_{AD} = 0,\quad Z_{AD} = D$
Case 3:	$D = H,\quad X_{AD} = 0,\quad Y_{AD} = \sigma,\quad Z_{AD} = D$
Case 4:	$D = H,\quad X_{AD} = -5H,\quad Y_{AD} = \sigma,\quad Z_{AD} = D$
Case 5:	$D = H/3,\quad X_{AD} = 0,\quad Y_{AD} = 0,\quad Z_{AD} = D$
Case 6:	$D = H/3,\quad X_{AD} = -5H,\quad Y_{AD} = 0,\quad Z_{AD} = D$
Case 7:	$D = H/3,\quad X_{AD} = 0,\quad Y_{AD} = \sigma,\quad Z_{AD} = D$
Case 8:	$D = H/3,\quad X_{AD} = -5H,\quad Y_{AD} = \sigma,\quad Z_{AD} = D$

Figure 28 is a side view showing the streamlines passing $\left(X_{AD}, Y_{AD}, Z_{AD} \pm \frac{D}{2}\right)$. Fuga and RANS give very similar results for both the large and the small actuator disk. The Fuga streamlines swing slightly less to the sides than the RANS streamlines in cases 3, 4, 7 and 8. The agreement is better for elevated streamlines than for streamlines closer to the ground, where the perturbations are larger. The RANS calculations took about 10 minutes per case while the Fuga calculations took about 5 seconds for all the cases.

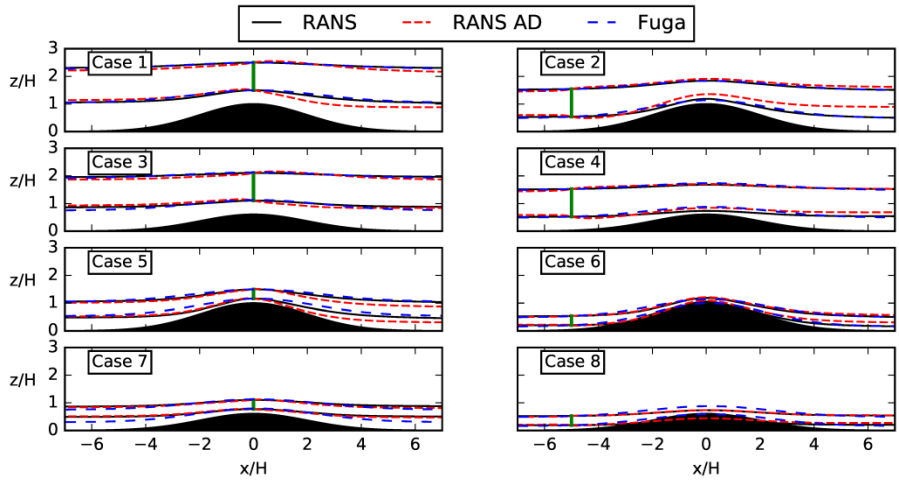

Figure 28: Flowlines over a Gaussian hill with side view.

Generalization of the DWM model to moderately complex terrain

Based on the generalization of the 'classic' Fuga model to moderately complex terrain conditions, the 'classic' DWM model has been generalized to the same type of non-homogeneous terrain (Larsen, 2017). This is done through adopting a suite of 5 conjectures, of which some are identical to simplifications done for the classic DWM formulation, and others are directed against the generalization to moderately complex terrain applications. These basic conjectures are:

Conjecture 1: Non-linear *shear interaction* with wakes is *not* considered.

Conjecture 2: The downstream advection of a wake is presumed to follow a certain *advection streamline* associated with free flow conditions - i.e. the flow field without wakes included. This is also the case for the 'classic' DWM model, but for flat and homogeneous terrain, the streamlines are just straight lines.

Conjecture 3: Wakes carry momentum, and these can therefore only with some modifications be considered to act approximately as passive tracers in the sense of kinematics. As for the wake deficit interaction with the inhomogeneous flow conditions along a streamline in a moderately complex terrain, we will assume that wake *expansion* is not significantly affected by hill speedup, and thus as a consequence assume that wake deficits along a streamline scales under a similarity presumption.

Conjecture 4: The wake *advection speed* along the *advection streamline* can be simplistically described as based on a Hill's vortex approach.

Conjecture 5: Wake meandering (laterally, vertically) around the *advection streamline* is assumed driven by large-scale Atmospheric Boundary Layer (ABL) turbulence. The large scale ABL segment is in the present context defined with a cut off frequency of U/2D in analogy with the 'classic' DWM model. It is further assumed, that conventional homogeneous anisotropic ABL turbulence for flat terrain , and expressed in a Cartesian frame of reference, can be used for the large scale turbulence driving the wake meandering.

In analogy with the 'classic' DWM model, the generalization of the DWM model to moderately complex terrain is based on a *deterministic* downstream advection of wake deficits superimposed by *stochastic* wake meandering in 2D planes perpendicular to the advection path. The main differences between the 'classic' DWM model and the DWM model for moderately complex terrain conditions relate to conjectures 2 and 3. We will briefly give a little insight to these and otherwise refer to (Larsen, 2018) for more details.

Adopting *conjecture 2*, the deterministic wake downstream advection path is chosen as a specific streamline. A wake deficit does, however, have a spatial extend, and consequently an infinity number of streamlines (or combination of such) are possible candidates. Contrary to flat and homogeneous terrain, the streamlines in moderately complex terrain converges and diverges, depending on the terrain geometry, and the definition of the particular advection streamline therefore actually matters for such terrains. It is difficult to set up a general definition as based on a specific metric, because even moderately complex terrains exhibit a huge variability of terrain geometries and thereby streamline behavior, but also because the streamlines for wake affected flows for a given complex terrain departs from the analog streamlines for the no-wake situation. This is because wakes - contrary to passive tracers - 'carry' momentum.

To motivate the definition of the advection streamline, a CFD RANS study was conducted for simple 2D Gaussian ridges, with the inflow being perpendicular to the ridge and the wake generating turbine represented by an actuator disc. Based on this study, it was concluded that choosing the wake deficit streamline at the *largest vertical distance* from the terrain surface as the advection streamline was superior to other choices. From a heuristic perspective, this makes sense, as the further we move from the terrain surface, the more unaffected are the streamlines of the terrain topology. The streamline characteristics thus asymptotically approach the flat-terrain case, where the particular streamline defined as the advection streamline does not matter. At this point, it should be mentioned that the present study is confined to *neutral* ABL conditions. Non-neutral ABL stratification is a study of its own, and under such conditions large impact on the streamlines is expected - cf. (Wildmann, 2018) for a full-scale study of such phenomena.

In analogy with the 'classic' DWM model, the quasi-steady wake deficit is described in the meandering frame of reference (MFoR). However, in addition to downstream wake diffusion and meandering, the quasi-steady wake deficit will, in the moderately complex terrain case, also be affected by the *spatially non-homogeneous* character of the average flow field - i.e. the spatial variability in the mean flow characteristics dictated by the terrain topology. This is because of the wake deficit being an organized flow structure carrying momentum. We have accounted for that in an approximate manner using *conjecture 3* in combination with a *wake similarity presumption* stating that the wake deficits expressed in MFoR scales with a parameter, ε, depending on the spatially dependent ambient mean wind speed, and a simple closed form expression of this scaling parameter has been derived.

Extension of the Jensen wake model for flows in complex terrain

The most widely used engineering wake model: Jensen wake model, has been adapted for applications in complex terrain. The original Jensen wake model was derived for wind turbines in flat terrain or offshore. To extend it for wind turbines in complex terrain, we make the following assumptions:

1) centerline of the wake zone behind a rotor follows the ground of terrain along the wind direction;
2) velocity deficit and radius of the wake zone develop linearly according to the traveling distance of the wake;
3) multiple wakes and/or partial wakes merged at each rotor satisfy the kinetic energy deficit balance assumption.

This adapted model was first presented in the TORQUE conference in 2014 (Feng and Shen, 2014) and is now used in the FarmOpt code. Consider two turbines in complex terrain: WT_i at location (x_i, y_i, z_i) and WT_j at location (x_j, y_j, z_j). Assuming wind blows along x direction and the wake of WT_i hits the rotor of WT_j , we can plot the wake development diagram as in Figure 29.

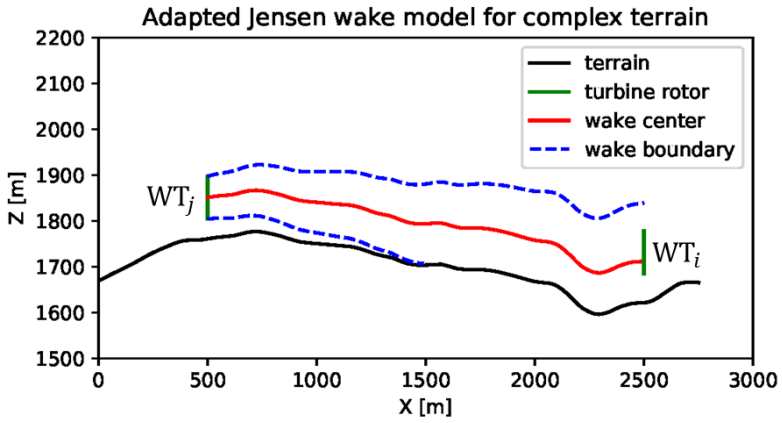

Figure 29: Schematic of the adapted Jensen wake model for wind turbines in complex terrain.

For a given combination of far field inflow wind speed V^{∞} and wind direction θ^{∞} at the hub height above the ground level, we can first transform the coordinates so that wind blows along the new x direction. Based on the first two assumptions described above, the wind

speed and the wake zone radius of the wake of WT_j when arriving WT_i, denoted as V_{ij} and R_{ij}, are obtained as:

$$V_{ij} = SP_j(\theta^{\infty})V^{\infty}\left[1 - \frac{1-\sqrt{1-C_T(SP_j(\theta^{\infty})V^{\infty})}}{\left(1+\alpha(s_{ij}/R_r)\right)^2}\right] \quad (1)$$

$$R_{ij} = \alpha s_{ij} + R_r \quad (2)$$

where $SP_j(\theta^{\infty})$ is the speed-up factor at the location of WT_j for far field inflow wind direction θ^{∞}, which is mainly induced by terrain effect, $C_T(\cdot)$ denotes the thrust coefficient of wind turbine (WT) at certain wind speeds, α is the wake decay coefficient, R_r represents the radius of rotor and s_{ij} is the curved distance between the 2 WTs along the wind direction, i.e., the red curve in Figure 29, which is calculated based on locations and terrain data.

On the transversal plane of WT_i's location ($x = x_i$), the rotor of WT_i and the wake zone of WT_j can be represented as two circles, with radius R_r and R_{ij} respectively, located at the same height. Depending on the transversal distance between their centres, which can be denoted as $d_{ij} = |y_i - y_j|$, the rotor of WT_i might be in full wake, in partial wake or out of wake of WT_j, as shown in Figure 30.

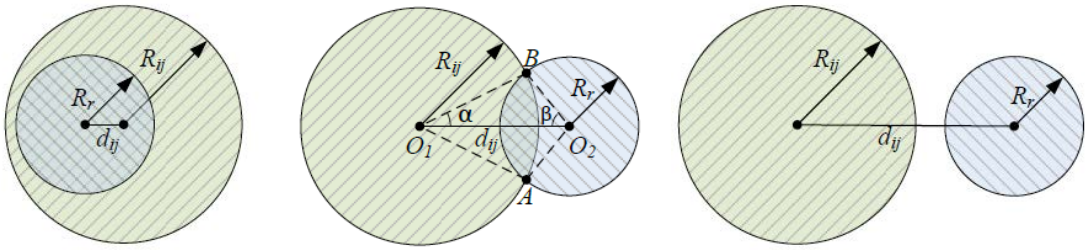

(a) $d_{ij} \le R_{ij} - R_r$ (b) $R_{ij} - R_r < d_{ij} < R_{ij} + R_r$ (c) $d_{ij} \ge R_{ij} + R_r$

Figure 30: Affected area of WT_i's rotor byWT_j's wake in: (a) full wake, (b) partial wake, (c) out of wake

Then the overlapping area A_{ij} can be easily calculated following the procedure described in (Feng and Shen 2014). Based on the third assumption, we can derive the effective wind speed WT_i experienced in a wind farm composed of N_{wt} WTs as follows:

$$\bar{V}_i = SP_i(\theta^{\infty})V^{\infty} - \sqrt{\sum_{j=1,j\neq i}^{N_{wt}}\left[\frac{A_{ij}}{A_r}\cdot\left(SP_j(\theta^{\infty})V^{\infty} - V_{ij}\right)\right]^2} \quad (3)$$

where $A_r = \pi R_r^2$ is the rotor area of WT.

Linking simplified wake models to detailed RANS CFD terrain models

To link the simplified wake model such as the adapted Jensen wake model with CFD terrain model, we need to extract the relevant information on terrain effect and wind resource from the CFD simulations, such as the inflow direction dependent speed-up factors for all turbine sites, which are used in Equations (2)-(3).

To do this, FarmOpt has built interfaces with WAsP and WindPRO, mainly utilizing the resource grid calculated in WAsP or WindPRO, which contains the sector-wise information for each grid on Weibull parameters, mean wind speed, speed-up factor, turning angle, etc. Either the traditional linear model (IBZ in the conventional WAsP) or a more advanced model such as WAsP CFD (an integrated part of WAsP designed for wind resource assessment in complex terrain) can be applied to calculate the resource grid.

FarmOpt extracts the relevant information on wind resource and terrain effects from the resource grid. FarmOpt then finds the required information for any location and under any given inflow wind direction by interpolation. Some of the interpolated values for a complex terrain site are shown in Figure 31.

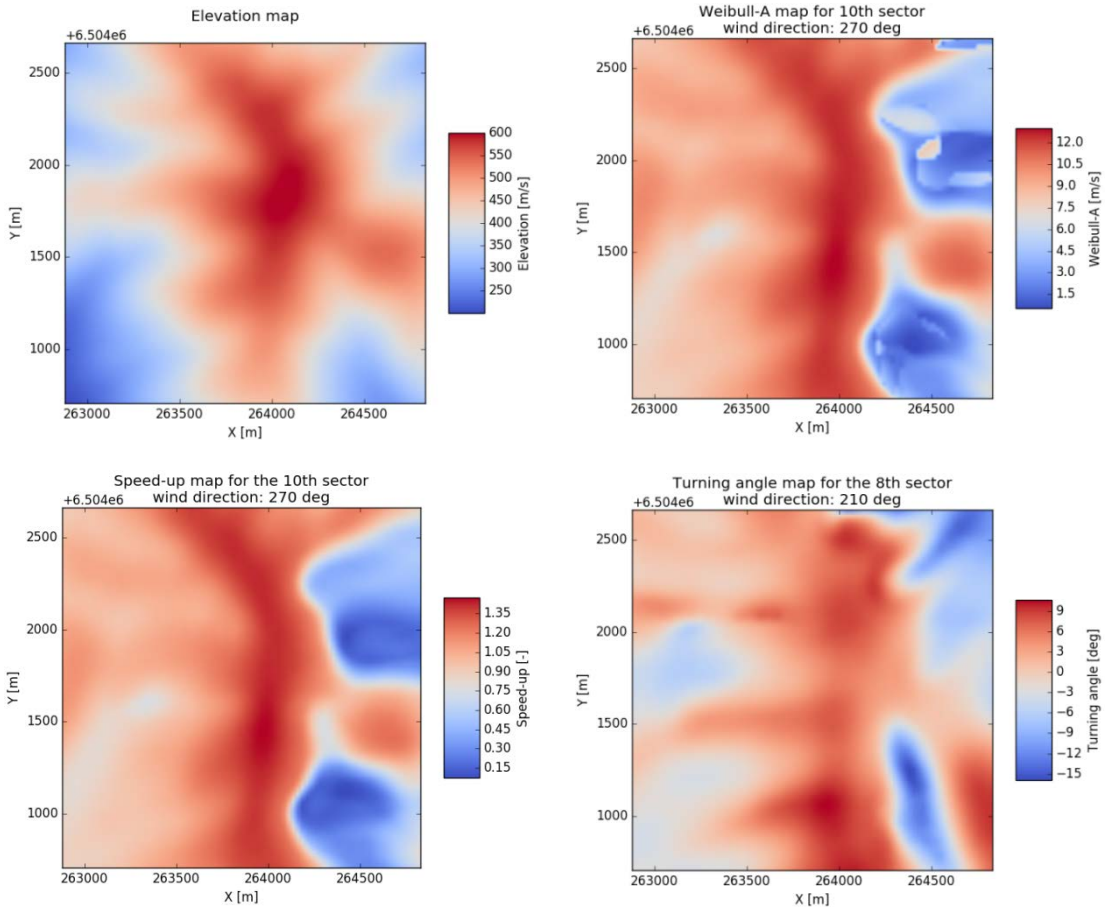

Figure 31: Terrain and wind resource information for a complex terrain site: (top-left) elevation; (top-right) Weibull-A parameter; (bottom-left) speed-up factor; (bottom-right) turning angle.

1.5.5 Wind farm layout tool (WP6)

WP6 contains 4 tasks: 1) Development of advanced optimization tools, 2) software integration, 3) small wind farm optimization and demonstration, and 4) large wind farm optimization and demonstration.

Development of advanced optimization tools

Objective function

The objective of wind farm design optimization can be many types, from maximizing annual energy production (AEP) to minimizing levelized cost of energy (LCOE), from single-objective to multi-objective. In its current and simplest version, FarmOpt formulates wind farm design as a single objective optimization problem, i.e., maximizing the AEP for a given wind farm by optimizing its layout with a given number of WTs. In other studies, different objectives were attempted for offshore wind farms: multi-objective (maximizing the mean power and minimizing the length of internal cables) in (Feng and Shen, 2016), maximizing robustness in (Feng and Shen, 2017) (1) and minimizing LCOE in (Feng and Shen, 2017) (2).

Constraint modelling

Wind farm design in complex terrain inevitably encounters various constraints and requirements, which might come from the considerations on wind resource, flow characteristics, terrain features, etc. FarmOpt includes a constraint module to account various constraints. Currently, it has modelled the constraints on mean wind speed, terrain ruggedness degree, inclusive zones, exclusive zones, and minimal distance requirements between any two WTs. Other constraints can be easily added. An example of such constraint modelling is shown in Figure 32.

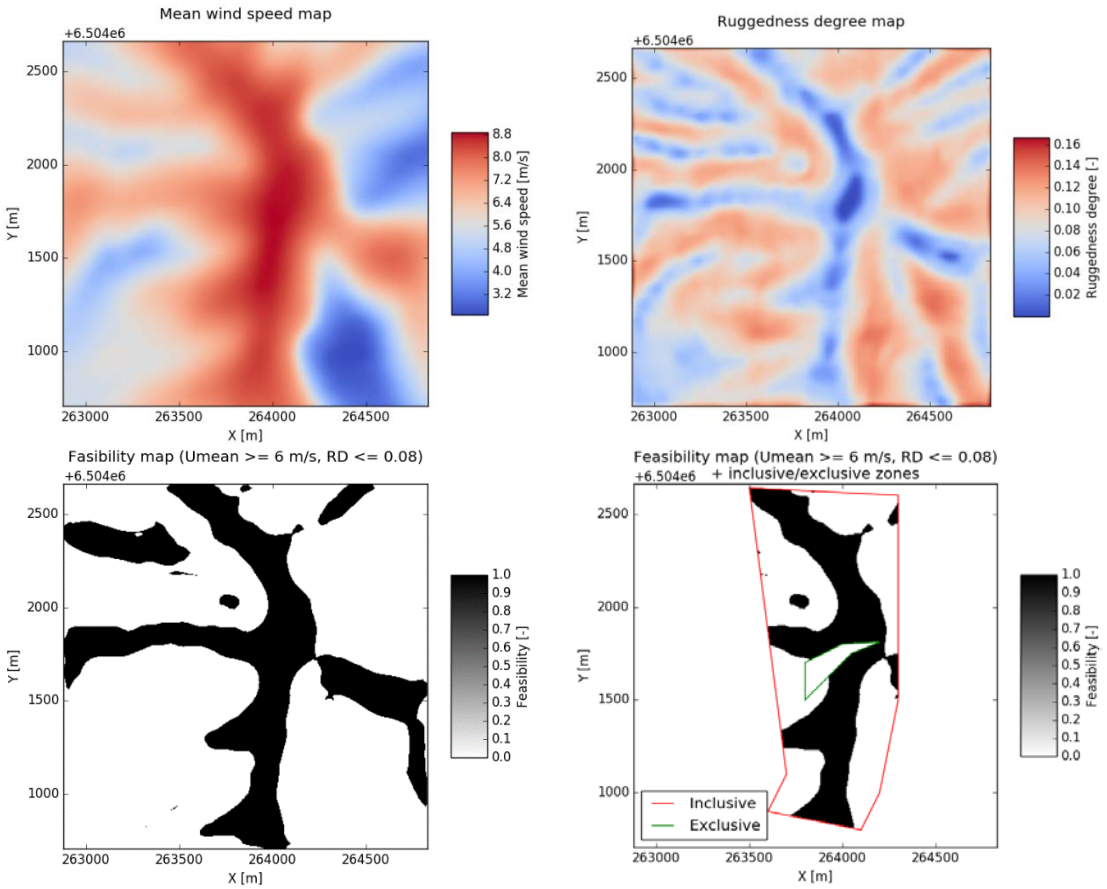

Figure 32: Constraint modelling of FarmOpt: (top-left) map of mean wind speed; (top-right) map of ruggedness degree; (bottom-left) constraints on minimal mean wind speed and maximal ruggedness degree; (bottom-right) adding constraints on inclusive zone and exclusive zone.

Optimization algorithm

In order to solve the wind farm design optimization problem, a family of Random Search algorithms has been developed. It is a single-solution based search algorithm, which iteratively generates new feasible solution that satisfies the constraints and keeps the improved one as the current best solution. The flowchart of the single-objective version of Random Search is shown in Figure 33. The details of the algorithm can be found in (Feng and Shen, 2015).

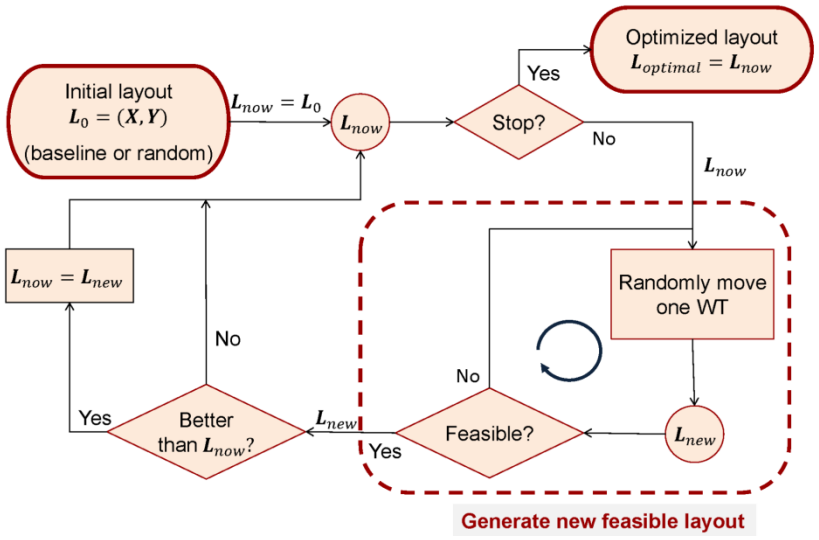

Figure 33: Flowchart of single-objective Random Search algorithm.

The algorithm has been tested on a wind farm of 25 WTs on a Gaussian hill for maximizing the total mean power. The initial and optimized layouts are shown in Figure 34. Note that in

this test case, the chosen wind turbine is Vestas V80 2.0MW turbine with rotor diameter of 80 m and the required minimal distance between any two turbines is set as 5 rotor diameters.

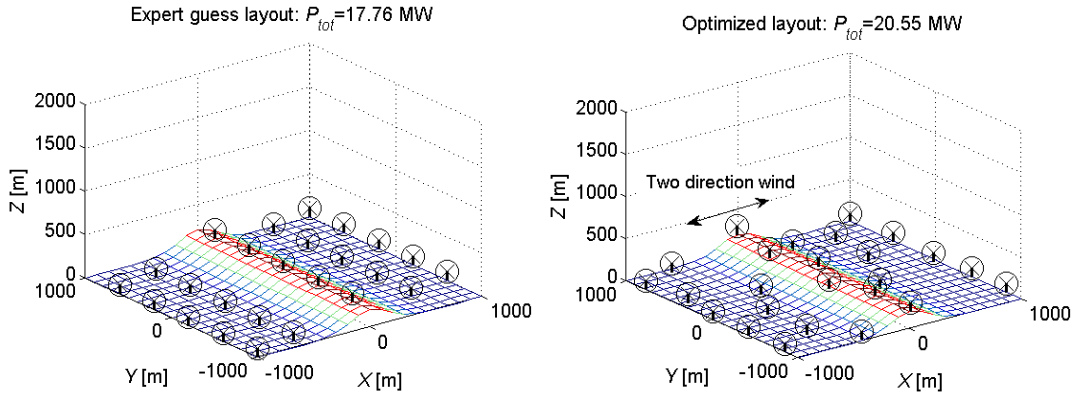

Figure 34: Initial guess and optimized layout of a wind farm on a Guassian hill with 25 wind turbines.

In the study presented in (Feng and Shen, 2015), the Random Search algorithm was compared with Genetic Algorithm (GA) for a widely studied ideal test case that was first proposed by Mosseti et al. The results showed that the Random Search algorithm outperforms GA in all 3 wind scenarios. When applied to a large offshore wind farm, i.e., the Horns Rev 1 wind farm, which is composed of 80 Vestas V80 2.0MW turbines, this algorithm also obtained solid and robust improvement for power production. Details of the results can be found in (Feng and Shen, 2015). It is also worthy to note that our first journal paper presenting the Random Search algorithm, i.e., (Feng and Shen, 2015), has been cited for 40 times according to Google scholar (25 times according to Web of Science) since its publication in 2015, clearly demonstrating its high influences among researchers in this field. The single objective Random Search algorithm shown in Figure 33 has also been extended to other scenarios and achieved promising performances when comparing with other popular competitive algorithms.

A multi-objective Random Search (MORS) algorithm was proposed to simultaneously maximize the power production and minimize the total length of electrical cables connecting all turbines. It was applied to the Horns Rev 1 wind farm and managed to find a group of Pareto optimal solutions. When compared with the most widely used multi-objective algorithm: NSGA-II (Non-dominated Sorting Genetic Algorithm II), it shows astonishingly better performance for the test case, i.e., managed to find much better Pareto frontiers even with far less evaluations, as shown in Figure 35. This work was presented as an oral presentation in the TORQUE 2016 conference.

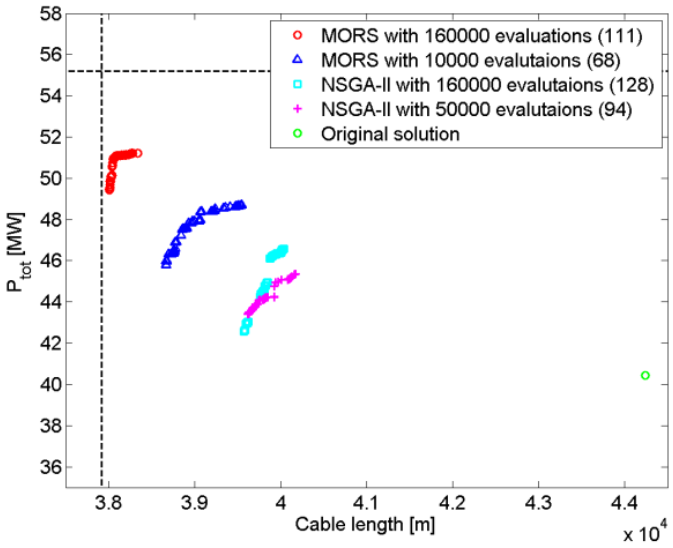

Figure 35: Comparison between different results obtained by MORS and NSGA-II (the number in brackets shows how many solutions are found in the final Pareto frontier)

In a recent study (Feng and Shen, 2017), the algorithm was also extended for mixed-integer-discrete optimization problems, by simultaneously optimizing the turbine locations, turbine types and number of turbines to minimize the LCOE of a given wind farm. This algorithm has been applied for an offshore wind farm and shown a much better performance when compared to the mixed-discrete particle swarm optimization (PSO) algorithm, as shown in Figure 36. Note that in this comparison, the algorithm described in (Feng and Shen, 2017) finds solutions that converge to a lower LCOE in multiple runs, while consuming much fewer evaluations. Details of this algorithm and its application can be found in (Feng and Shen, 2017).

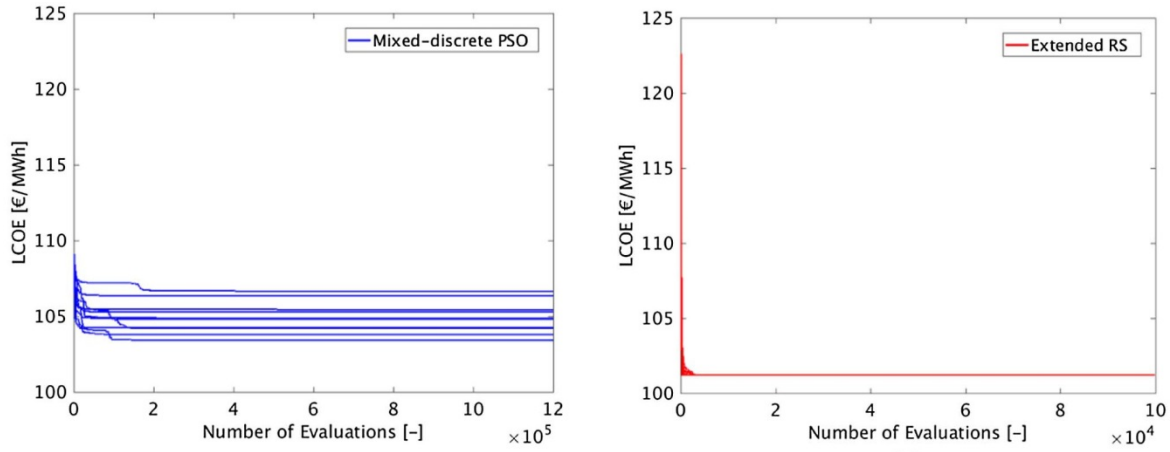

Figure 36: Performance of mixed-discrete PSO (left) and extended random search (right) in 10 optimization runs for an ideal test case.

To consider the non-uniform wind farm design optimization in complex terrain, i.e., wind farms composed of different types of turbines with unfixed number of turbines, the extended random search algorithm will be a strong candidate.

Software integration

The flowchart of the FarmOpt methodology is shown in Figure 37.

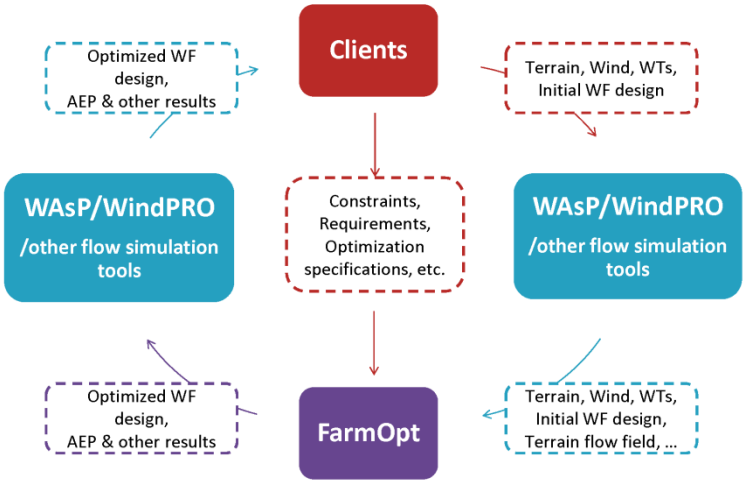

Figure 37: Flowchart of the FarmOpt methodology.

FarmOpt models the flow field by adding wake effects on top of the terrain flow field obtained by using existing industry standard wind resource assessment tools such as WAsP/WAsP CFD or WindPRO. Then the design optimization problem is solved by using advanced wind farm optimization algorithms, such as Random Search. Realistic constraints or requirements specified by the clients, typically wind farm (WF) developers, are also considered, such as constraints on WF boundary, exclusive zones, terrain ruggedness degree, minimal distance between WTs, minimal mean wind speed, and so on.

In order to integrate with WAsP and WindPRO, FarmOpt has an interface to work with the GIRAFFA IO format, which is a generalized i/o-format for adapting optimization frameworks for wind farm applications defined by EMD.

Currently, it can initialize a wind farm optimization problem from the .optireq file and conduct the layout optimization using random search. All the constraints on areas (inclusive and exclusive) and number of turbines, requirements on type of turbines are considered. The original and optimized layouts, together with the evolution history of optimization, are saved in .txt files and figures.

The architecture of the FarmOpt code can be described by the diagram in Figure 38. Note that besides some standard python modules, such as numpy, scipy and mathplot, FarmOpt also depends on some Python modules that are not as standard, and thus may need to be installed first, such as zipfile, xml and shapely.

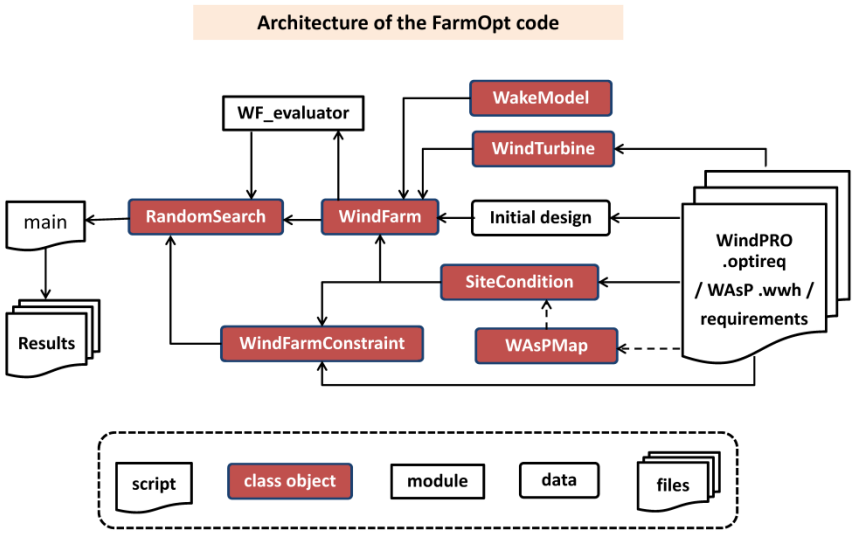

Figure 38: Architecture of the FarmOpt code.

The details of the software integration and a demonstration case using the GIRAFFA IO format are described in an internal report.

Small wind farm optimization and demonstration

A small wind farm in complex terrain composed of 8 wind turbines is considered. The terrain and wind resource information is as shown in Figure 31, and the constraint modelling aspect has been demonstrated in Figure 32. The optimization results are shown in Figure 39.

FarmOpt is used to optimize this small wind farm to maximize its AEP. With 1000 evaluations and considering two different minimal distance requirements (2 and 3 rotor diameters, D), the optimized layouts as shown in Figure 39 can yield substantial improvements in AEP: 3.72% for the 2D minimal distance and 1.14% for the 3D minimal distance.

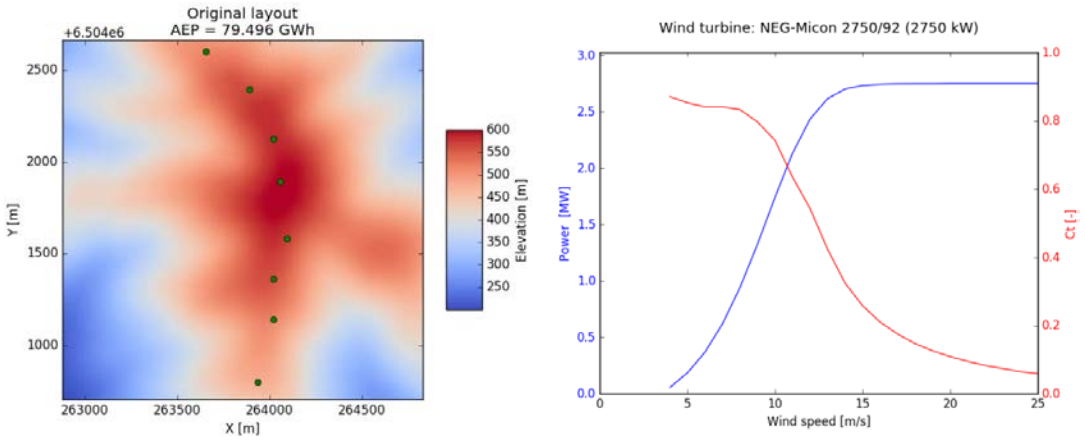

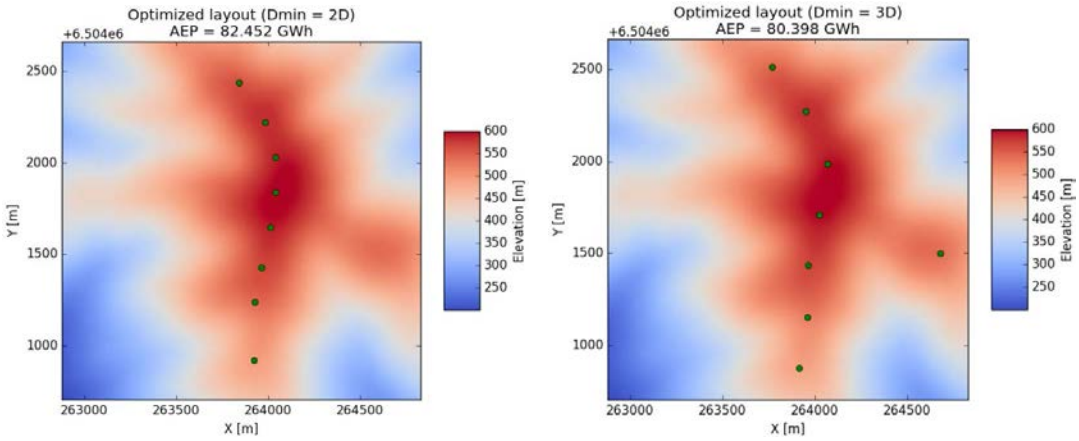

Figure 39: Optimizing a small wind farm in complex terrain: (top-left) the original layout; (top-right) WT characteristics; optimized layout for 2D (bottom-left) and 3D (bottom-right) minimal distance.

Large wind farm optimization and demonstration

A large wind farm with 25 turbines in complex terrain is considered. The constraints considered include the minimal polygon enclosing all the turbines, requirements on the minimal mean wind speed (6 m/s), maximal ruggedness degree (0.08), and minimal distance between turbines (4.34 D, i.e. the minimal value in the original layout). This wind farm is optimized using FarmOpt with 5,000 evaluations. The original layout, feasibility map, optimized layout and the evolution history are shown in Figure 40. The net AEP of the wind farm is increased from 161.839 GWh to 164.196 GWh, representing a 1.46% improvement. The CPU time is 63 278 s, when running on a Dell laptop from 2012 with Intel i5 CPU.

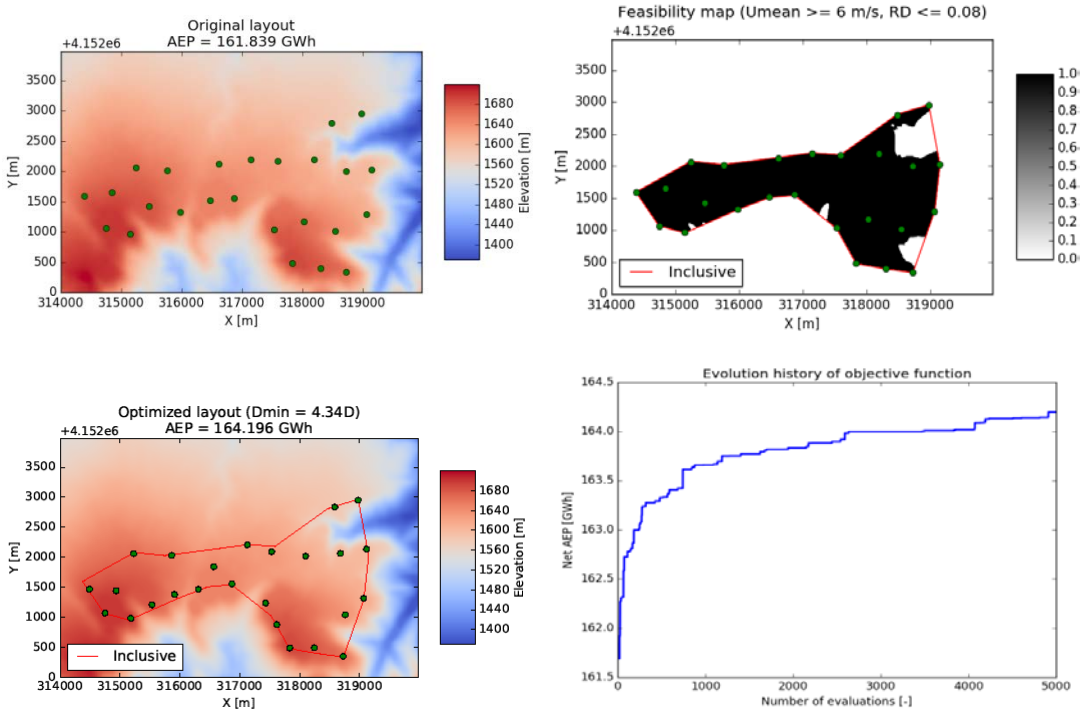

Figure 40: Optimizing a large wind farm in complex terrain: (top-left) the original layout; (top-right) feasibility map; (bottom-left) optimized layout; (bottom-right) evolution history.

As shown by the results of both small and large wind farms, FarmOpt is able to optimize wind farms in complex terrain, considering various realistic constraints and achieving substantial AEP improvements. This result together with the general methodology of FarmOpt was presented as an invited oral speak in the China Wind Power 2017 conference, which is the largest annual wind power exhibition in China. This speech attracted many interests from the conference attendants, who were mostly Chinese wind power industrial practitioners.

1.5.6 Software commercialization (WP7)

WP7 has 2 tasks: 1) Evaluation of existing commercial software, and 2) commercialization of the new software.

Evaluation of existing commercial software

In this project, WAsP CFD and WindPRO are the baseline tools for wind farm layout optimization. In order to evaluate existing commercial software as compared to the proposed ones, benchmark test cases are defined in Table 1 using the measured data in the Jingbian wind farm. The software and codes employed for the benchmark computations include WAsP, WAsP CFD, WindPRO, Meteodyn WT, WindSim and RANS/AD models.

The computational features are summarized below:

- Commercial software WAsP is a linearized flow solver based on the BZ model of Troen (1990). The computational domain is 25 km x 25 km x 1 km where the last number is the height and meshed with 1 million points and the finest mesh size of 4 m.
- Commercial software WAsP CFD is based on the incompressible Navier-Stokes solver EllipSys3D. The computational domain is a cylinder with a radius of 34 km and height of 14 km. The center domain is 6 km x 4 km. The total mesh has 7 million points and a finest resolution of 5 m in the vertical direction and 20 m in the horizontal direction. The used turbulence model is k-ε model.
- Commercial software WindPRO is based on WAsP CFD and has a similar mesh resolution.
- Commercial software Meteodyn WT is a CFD-based code. The computational domain is a cylinder with a radius of 34 km and height of 14 km. The center domain is 5.5 km x 5.5 km. The total mesh has 6 million points and a finest resolution of 5 m in the vertical direction and 30 m in the horizontal direction.
- Commercial software WindSim is a CFD-based code interface that relies on the 3rd party Phoenix solver. The computational domain is a cylinder with a radius of 13.5 km and height of 2.5 km. The center domain is 5.5 km x 5.5 km. The total mesh has 6 million points and a finest resolution of 10 m in the vertical direction and 30 m in the horizontal direction. The used turbulence model is k-ε RNG model.
- RANS/AD is a Reynolds averaged Navier-Stokes and actuator disc model based on the incompressible Navier-Stokes solver EllipSys3D. The computational domain is a cylinder with a radius of 28 km and height of 25 km. The center domain is 7.8 km x 7.8 km. The total mesh has 31 million points and a finest resolution of 2.5 m in the vertical direction and 16 m in the horizontal direction. The used turbulence model is k-ε model.

To validate the codes, the flow case 1.4 with a wind speed of 7 m/s and a wind direction of 180° is considered. To estimate the ground effects, the front 9 turbines (No. 03, 07, 08, 10, 12, 14, 17, 18) are first considered. The comparisons are shown in Figure 41 and Table 7 (Mean_RE is absolute mean relative error; Tot_RE is total relative error). It is seen that WAsP CFD and WindPRO compare better with the measured data (SCADA) than the other codes.

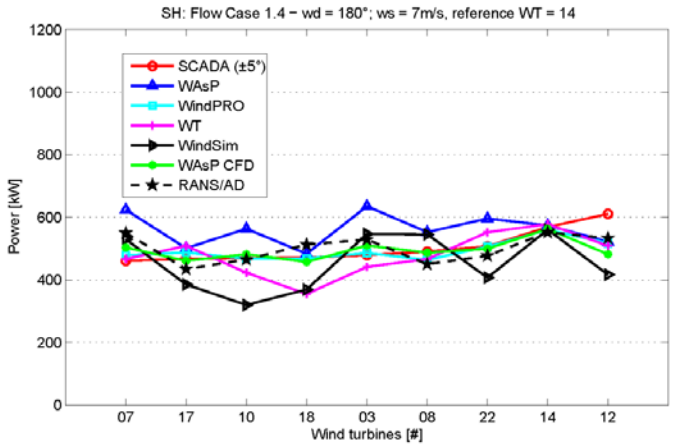

Figure 41: Comparison of power performance of the front turbines predicted with different codes for flow case 1.4.

Table 7: Comparison of mean and total power performance of the front turbines predicted with different codes for flow case 1.4.

	Mean_RE (%)	Tot_RE (%)
WAsP	15.96	11.64
WindPRO	3.66	1.95
WT	9.40	4.95
WindSim	18.27	9.81
WAsP CFD	5.26	1.76
RANS/AD	8.50	0.49

When all the turbines are considered, the comparisons are shown in Figure 42 and Table 8. From the figure and table, it is seen that the differences are larger. On the other hand, all the codes are seen to give very similar results. Note that in the south direction the terrain is very complex, and thus it is difficult to perform computations with uniform inflow conditions.

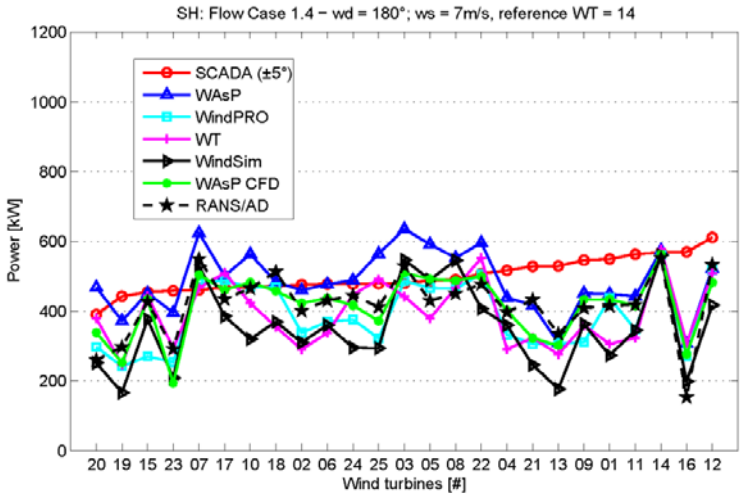

Figure 42: Comparison of power performance predicted with different codes for flow case 1.4.

Table 8: Comparison of mean and total power performance predicted with different codes for flow case 1.4.

	Mean_RE (%)	Tot_RE (%)
WAsP	16.80	2.69
WindPRO	22.84	22.34
WT	22.68	21.45
WindSim	32.37	29.47
WAsP CFD	17.82	16.70
RANS/AD	18.80	16.16

To check code performance in other directions, flow case 1.6 with a wind speed of 7 m/s and a wind direction of 330^{o} is studied. Flow case 1.6 is one of the main wind directions at the site. The comparisons are shown in Figure 43 and Table 9. From the figure and table, it is seen that all the codes give reasonable predictions on total and mean power output. WAsP CFD provides the closest match to the measured data (SCADA).

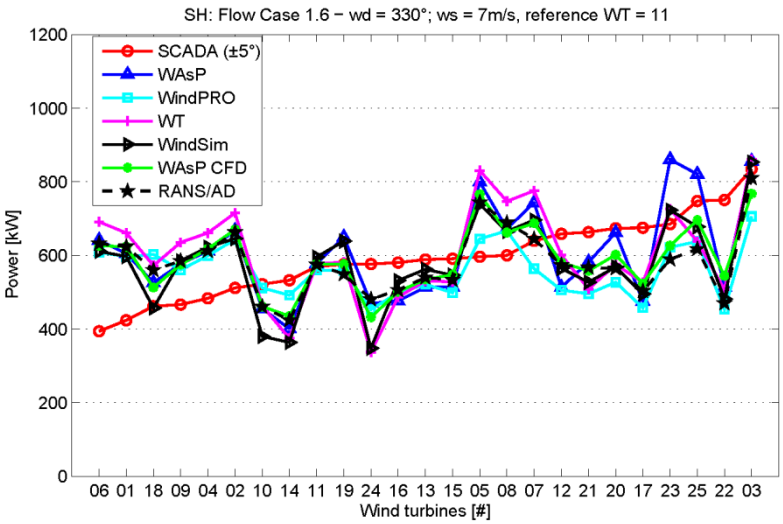

Figure 43: Comparison of power performance predicted with different codes for flow case 1.6.

Table 9: Comparison of mean and total power performance predicted with different codes for flow case 1.6.

	Mean_RE (%)	Tot_RE (%)
WAsP	20.46	2.58
WindPRO	19.40	5.51
WT	23.99	2.11
WindSim	19.44	2.19
WAsP CFD	17.75	0.66
RANS/AD	19.07	1.93

Commercialization of the new software

To efficiently commercialise the complex terrain CFD model (see section 1.5.2), an effort has been made to implement the changes directly in the WAsP and WindPRO software by DTU and EMD. Implementing the changes directly in the software will make the software more readily available for all existing customers.

The main technical addition to the two software programs is the inclusion of modelled ambient turbulence to the WAsP CFD results. The turbulence is needed to make layout optimisation based on the levellized cost of energy, i.e. an optimisation that considers both wind turbine production and lifetime costs. To integrate the turbulence, EMD has developed an open XML-based CFD and optimization interface, and the graphical user interfaces of both WindPRO and WAsP has been updated. The XML based open formats are described in technical reports by EMD, see (Thøgersen and Sørensen 2017, 2018) and (Sørensen, 2016).

To support the new additions in WAsP and WindPRO, the use of CFD has from 2015 been included in the WAsP courses and a master thesis. In addition, internal training at DTU has also been conducted.

1.5.7 New wind farm development (WP8)

As the wind farm design institute, NWI used the developed tools to design 5 Chinese wind farms in complex terrain in 2017 in collaboration with wind farm developers. The list of wind farms is listed in Annex 1.

1.5.8 Dissemination

The dissemination of results is mainly the publications in international journals and conferences, which are listed below:

Journal Publications with peer-review:

1. JF Herbert-Acero, O Probst, PE Réthoré, GC Larsen, and KK Castillo-Villar, "A Review of Methodological Approaches for the Design and Optimization of Wind Farms", Energies 2014, 7(11), 6930-7016; doi:10.3390/en7116930.

2. J Feng and WZ Shen, "Modelling Wind for Wind Farm Layout Optimization Using Joint Distribution of Wind Speed and Wind Direction", Energies 2015, 8(4), 3075-3092; doi:10.3390/en8043075.

3. LL Tian, WJ Zhu, WZ Shen, N Zhao, and WZ Shen, "Development and validation of a new two-dimensional wake model for wind turbine wakes", Journal of Wind Engineering & Industrial Aerodynamics, 2015, vol. 137, pp. 90-99.

4. J Feng and WZ Shen, "Solving the wind farm layout optimization problem using random search algorithm", Renewable Energy 2015, vol. 78, pp. 182-192.

5. LÉ Boudreault, A Bechmann, L Tarvainen, L Klemedtsson, L Shendryk, and E Dellwik, "A LiDAR method of canopy structure retrieval for wind modeling of heterogeneous forests", Agricultural and Forest Meteorology, 201:86-97, 2015. DOI: http://dx.doi.org/10.1016/j.agrformet.2014.10.014.

6. T Koblitz, A Bechmann, A Sogachev, NN Sørensen, and PE Réthoré, "Computational Fluid Dynamics model of stratified atmospheric boundary-layer flow", Wind Energy, 18:75-89, 2015. DOI: http://dx.doi.org/10.1002/we.1684.

7. E Machefaux, GC Larsen, N Troldborg, M Gaunaa, and A Rettenmeier, "Empirical modeling of single-wake advection and expansion using full-scale pulsed LiDAR-based measurements", Wind Energy 2015; 18: 2085–2103.

8. C Xu, X Han, X Wang, D Liu, Y Zheng, WZ Shen, and M Zhang, "Study of wind turbine wake modeling based on a modified actuator disk model and extended k-ε turbulence model", Zhongguo Dianji Gongcheng Xuebao 2015, Vol 35 (8), pp. 1954-1961, DOI:10.13334/j.0258-8013.pcsee.2015.08.015.

9. C Xu, CQ Li, XX Han, WZ Shen, MM Zhang, DY Liu, and Y Zhen, "Numerical simulation of the aerodynamic field in complex terrain wind farm based on actuator disk model", Journal of Engineering Thermophysics 2015, vol. 36, p. 1696-1700.

10. XX Han, C Xu, DY Liu, WZ Shen, Y Zhen, and MM Zhang, "Actuator disk model of wind farms based on the rotor average wind speed", Journal of Engineering Thermophysics 2016, vol. 37, pp. 501-506.

11. J Feng and WZ Shen, "Wind farm power production in the changing wind: Robustness quantification and layout optimization", Energy Conversion and Management 2017, vol. 148, 905-914.

12. J Feng and WZ Shen, "Design optimization of offshore wind farms with multiple types of wind turbines", Applied Energy 2017, vol. 205, 1283-1297.

13. H Zhou, C Xu, X Han, WZ Shen, M Zhang, and X Chen, "Numerical study of wind turbine wake modeling based on an actuator surface model", Journal of Engineering Thermophysics, 2017, Vol 38, Issue 3, p. 535-540.

14. X Han, D Liu, C Xu, and WZ Shen, "Experimental study of atmospheric stability effects on wind turbines in complex terrain", Renewable Energy 2018, In Press, https://doi.org/10.1016/j.renene.2018.03.048.

15. M Sessarego, WZ Shen, KS Hansen, P van der Laan, and WJ Zhu, "CFD simulations of

a wind farm in complex terrain and comparisons to measurements", submitted to Applied Sciences, 2018.

Conference publications, reports and presentations:

16. J Feng and WZ Shen. "Wind farm layout optimization in complex terrain: A preliminary study on a Gaussian hill". Journal of Physics 2014, vol. 524, 012151, 10 pages, doi:10.1088/1742-6596/524/1/012146.

17. LL Tian, WJ Zhu, WZ Shen, JN Sørensen, and N Zhao. "Investigation of modified AD/RANS models for wind turbine wake predictions in large wind farm". Journal of Physics 2014, vol. 524, 012151, 10 pages, doi:10.1088/1742-6596/524/1/012151.

18. XY Li, "Modelling of wind turbine wakes in complex terrain based on the results from CFD", Master thesis 2015, DTU Wind Energy.

19. D Kompolias, "Accurate and fast prediction of wind turbine performance in wind farm for layout optimization", Master thesis, 2015, DTU Wind Energy.

20. I Troen and BO Hansen, "Wind resource estimation in complex terrain: prediction skill of linear and nonlinear micro-scale models." In Orlando Orange County Convention Center 2015, United States.

21. A Sogachev, D Cavar, A Bechmann, and HE Jørgensen, "Assessment of consistent two-equation closure for forest flows", EWEA Annual Conference and Exhibition 2015, Paris, France.

22. KS Hansen, GC Larsen, R Menke, N Vasiljevic, N Angelou, J Feng, WJ Zhu, A Vignaroli, W Liu W, C Xu, and WZ Shen, "Wind turbine wake measurement in complex terrain", Journal of Physics: Conference Series 753 (2016) 032013, doi:10.1088/1742-6596/753/3/032013, 10 pages.

23. J Feng, WZ Shen, and C Xu, "Multi-objective random search algorithm for simultaneously optimizing wind farm layout and number of turbines", Journal of Physics: Conference Series 753 (2016) 032011, doi:10.1088/1742-6596/753/3/032011, 11 pages.

24. C Xu, D Chen, X Han, H Pan, and WZ Shen, "The collection of the main issues for wind farm optimisation in complex terrain", Journal of Physics: Conference Series 753 (2016) 032066, doi:10.1088/1742-6596/753/3/032066, 12 pages.

25. L Svenningsen, C Schmitt, and G Potzka, "Accuracy of load assessments based on modelled turbulence - the German example." In Wind Europe Summit 2016, Vol. Abstract ID: 309 Poster code: PO.253, Hamburg, Germany.

26. A Bechmann, "Perdigão CFD grid study", DTU Wind Energy 2016, E 0120.

27. TG Sørensen, "FLOWRES: Generalized flow request and result format", EMD International A/S, 2016.

28. KS Hansen, "Project FarmOpt – WP2 Data transfer – internal working", document dated 21/1-2016.

29. J Feng and WZ Shen, "Wind farm design in complex terrain - the FarmOpt methodology", Invited speaker at China Wind Power 2017.

30. GC Larsen, S Ott, and P van der Laan, "A framework for medium-fidelity wake dynamics in moderately complex terrain", Symposium on Wind Farm Siting in Complex Terrain 2017, Beijing, China, October 20, 2017.

31. ML Thøgersen and TG Sørensen, "SITERES: Generalized gridded results format for wind farm site and climate parameters", EMD International A/S, 2017.

32. ML Thøgersen and TG Sørensen, “GIRAFFA: Generalized I/O-format for Adapting Optimization Frameworks for Windfarm.-Appliations”, EMD International A/S, 2018.

33. GC Larsen, S Ott, and P van der Laan, “Medium-fidelity modeling of unsteady flows under complex terrain topologies”, to appear, 2018.

34. N Wildmann, S Kigle, and T Gerz, “Coplanar LiDAR measurement of a single wind energy converter wake in distinct atmospheric stability regimes at the Perdigão 2017 experiment”, Conference of The Science of Making Torque from Wind 2018.

Symposium

A symposium on wind farm siting in complex terrain was organized in Beijing on October 20th, 2017 with participants from both the Danish and Chinese partners and some guests from Goldwind, Mingyang Wind Power, CRRC Wind, etc. The program is attached in Annex 2.

1.6 Utilization of project results

DTU Wind Energy is the coordinator of the EUDP project. As DTU is a university, the results obtained in the project, especially the measurement data in wind farm in complex terrain, and the new wind farm design tools and computational methods considered as the state-of-the-art in developing wind farms in complex terrain, will be further used for future research or projects in the same area.

EMD International A/S is the industrial partner of the project. The FarmOpt project has given a substantial upgrade to the commercial software WindPRO for current and future commercialization. While a number of developments (CFD, parts of the EMD-LOAD RESPONSE and optimization) have been implemented in the software throughout the project, these developments are to be seen as a solid platform that will enable additional features to be more easily implemented – and to give an advantage over other commercially competing products.

1.7 Project conclusion and perspective

The project has been completed successfully. The main results include the 1-year measurement data in a wind farm in complex terrain, new wind farm optimization tools, the integration of the new wind farm optimization design tools with the commercial software WindPRO and WAsP, and the use of the obtained results into new wind farm developments, which have been described briefly in Subsections 1.5.1-1.5.8.

As the current project mainly focuses on the design of highly efficient and low cost wind farms in complex terrain, the future focus will be the development of low noise wind farms.

For EMD, the successful co-operation between project partners and the successful completion of the project has meant that valuable knowledge developed within the project has been activated in the planning and development of new features in windPRO. These activities cover flow modelling (CFD), dynamic wakes, relevant environmental impact and their link to complex terrain optimizations. The first part of these commercially available new features within optimization has been included for beta users of windPRO 3.2 since ultimo 2017 – with final commercial release in windPRO 3.2 planned for primo 2018. This includes including generalized optimization request and result format (GIRAFFA) - as well as a cloud based optimization service and infrastructure (currently accessed in a simplified way from http://farmopt.emd.dk). Next steps – partly build on FarmOpt technology - will be to more constraints into the optimization method – including constraints from structural loads, environmental impacts and cost-of-energy. These features – partly based on FarmOpt gained knowledge - is scheduled for next release of windPRO (3.3 – expected ultimo 2018)

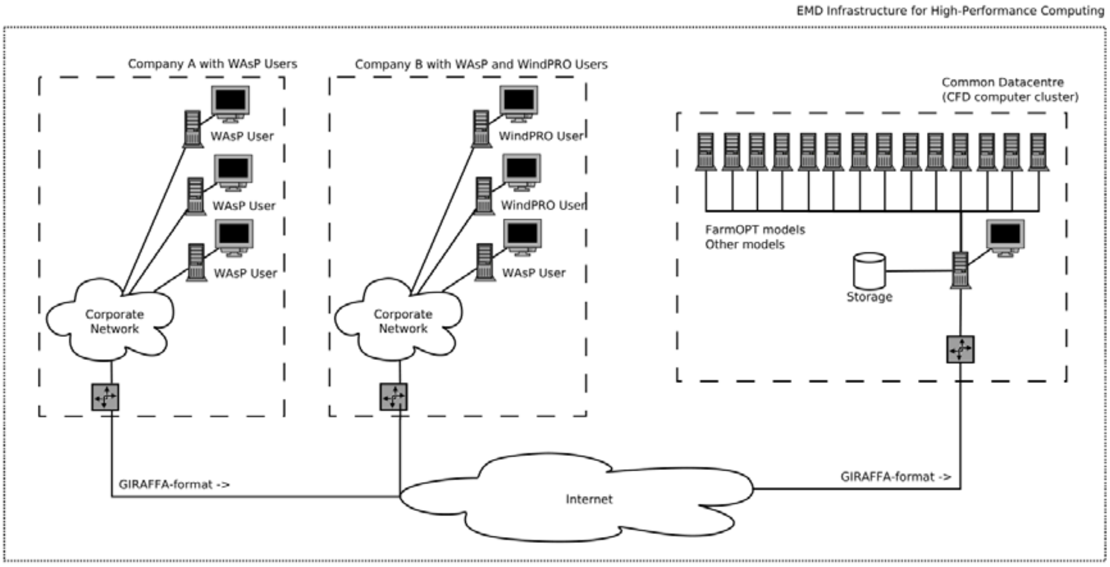

Figure 44: EMD Infrastructure and High Performance Computer Cluster for Optimization.

Annex 1: Certificate of erecting new wind farms in complex terrain

NWI developed new wind farms in complex terrain using the tools developed in the FarmOpt project. These new wind farms are

- The wind farm of Zhongwei Xiangshan with 50 MW erected in collaboration with National Electric Ningxia New Energy Corporation, built in August 2017 (top-left figure).
- The wind farm of Yanchima Wangshan with 50 MW erected in collaboration with National Electric Ningxia New Energy Corporation, built in August 2017 (top-right figure).
- The wind farm of Lijialiang with 50 MW erected in collaboration with Yellowriver Energy Corporation in Jingbian, built in September 2017 (mid-left figure).
- The wind farm of White Swan with 50 MW erected in collaboration with Yellowriver Energy Corporation in Jingbian, built in September 2017 (mid-right figure).
- The wind farm of Longzhou with 50 MW erected in collaboration with National Electric Jingbian Corporation in Jingbian, built in October 2017.

应用证明

靖边县黄河能源有限责任公司靖边李家梁风电场 50MW 工程在设计阶段，应用中国电建集团西北勘测设计研究院有限公司开发的风资源和微观选址优化软件，经后期运行比对，风资源计算准确，风机的机位属于全场优化的机位，机组运行状况优良。

靖边县黄河能源有限责任公司风电项目部

2017 年 9 月 20 日

应用证明

国电电力宁夏新能源开发有限公司所属宁夏中卫香山韩家圈风电场 50MW 工程设计阶段，应用中国电建集团西北勘测设计研究院有限公司开发的风资源和微观选址优化软件，经后期运行比对，风资源计算准确，风机的机位属于全场优化的机位，机组运行状况优良。

特此证明

国电电力宁夏新能源开发有限公司

2017 年 8 月 20 日

应用证明

国电电力宁夏新能源开发有限公司所属宁夏盐池麻黄山风电场一期 50MW 工程设计阶段，应用中国电建集团西北勘测设计研究院有限公司开发的风资源和微观选址优化软件，经后期运行比对，风资源计算准确，风机的机位属于全场优化的机位，机组运行状况优良。

特此证明

国电电力宁夏新能源开发有限公司

2017 年 8 月 25 日

应用证明

靖边县黄河能源有限责任公司靖边白天赐风电场 50MW 工程在设计阶段，应用中国电建集团西北勘测设计研究院有限公司开发的风资源和微观选址优化软件，经后期运行比对，风资源计算准确，风机的机位属于全场优化的机位，机组运行状况优良。

靖边县黄河能源有限责任公司风电项目部

2017 年 9 月 25 日

应用证明

华能陕西靖边电力有限公司龙洲风电场 50MW 工程在设计阶段，应用中国电建集团西北勘测设计研究院有限公司开发的风资源和微观选址优化软件，经后期运行比对，风资源计算准确，风机的机位属于全场优化的机位，机组运行状况优良。

华能陕西靖边电力有限公司

2017 年 10 月 27 日

Annex 2:

Symposium on Wind Farm Siting in Complex Terrain

Date: Friday, October 20, 2017; Address: Andeli N St 21 (安德里北街， Chuan You Hotel (川油宾馆)), Beijing, China

Time	Activities	
10:00 – 10:10	**Meet and Prepare / Welcome Coffee**	
10:10 – 10:20	Welcome	Chief Engineer Wei Liu, *PowerChina, Xibei Engineering Corporation Limited* Prof Wen Zhong Shen, *Technical University of Denmark (DTU)*
	Session 1: Wind Turbine Wakes, chaired by Wen Zhong Shen (DTU)	
10:20 – 10:45	Wind turbine wake measurements in complex terrain	Senior Researcher Kurt S. Hansen *Technical University of Denmark (DTU)*
10:45 – 11:10	Medium fidelity modeling of non-stationary wake affected flow fields under non-neutral ABL stability conditions	Senior Researcher Gunner Chr. Larsen *Technical University of Denmark (DTU)*
11:10 – 11:35	Experimental study of atmospheric stability effects on wind turbines in complex terrain	Feifei Xue *HoHai University (HHU)*
11:35 – 12:00	Data analysis of aerodynamic measurements in complex terrain	Hongliang Yuan *PowerChina, Xibei Engineering Corporation Limited*
12:00 – 13:00	**Lunch**	
	Session 2: Wind Farms, chaired by Chang Xu (HHU)	
13:00 – 13:25	Predictions of wind farm performance in complex terrain	Prof Wen Zhong Shen *Technical University of Denmark (DTU)*
13:25 – 13:50	Research on wind profiles effected by atmospheric stability and topographical condition	*Yi Hu* *PowerChina, Xibei Engineering Corporation Limited*
13:50 – 14:15	Offshore wind energy resource assessment	Feifei Xue *HoHai University (HHU)*
14:15 – 14:40	Wind turbine blade root loss innovation based on hybrid numerical methods	Prof Wei Jun Zhu *Yang Zhou University (YZU)*
14:40 – 15:10	**Coffee Break**	
	Session 3: Wind Farm Design, chaired by Morten Thøgersen (EMD)	
15:10 – 15:35	Wind farm optimization in complex terrain using windPRO – methods and case study	Dr Morten Thøgersen *EMD International (EMD)*
15:35 – 16:00	Wind farm design in complex terrain: wake modeling and layout optimization	Researcher Ju Feng *Technical University of Denmark (DTU)*
16:00 – 16:25	Wind farm design and optimization software development	Professor Chang Xu *HoHai University (HHU)*
16:25 – 16:50	How national noise code requirements impact the layout of wind farms	Dr. Thomas Sørensen *EMD International (EMD)*
16:50 – 17:00	**Closing Remarks**	